



Published in final edited form as:

Arterioscler Thromb Vasc Biol. 2023 August ; 43(8): e339–e357. doi:10.1161/ATVBAHA.123.319145.

Redox Dysregulation of Vascular Smooth Muscle Sirtuin-1 in Thoracic Aortic Aneurysm in Marfan Syndrome

Budbazar Enkhjargal, MD, PhD^{1,*}, Sandra Sulser Ponce De Leon, MSc^{1,*}, Yuko Tsukahara, PhD^{1,*}, Hanxiao Liu, BSc¹, Yuhao Huangfu, MSc¹, Yu Wang, BSc¹, Pedro Maria Seabra, MSc¹, Xiaoqi Yang, BSc¹, Jena Goodman, PhD¹, Xueping Wan, PhD¹, Vipul Chitalia, MD, PhD², Jingyan Han, PhD^{1,#}, Francesca Seta, PhD^{1,#}

¹Vascular Biology Section, Department of Medicine, Boston University School of Medicine, Boston, MA, USA

²Renal Section, Department of Medicine, Boston University School of Medicine, Boston, MA, USA

Abstract

Background: Thoracic aortic aneurysms (TAA) are abnormal aortic dilatations and a major cardiovascular complication of Marfan syndrome (MFS). We previously demonstrated a critical role for vascular smooth muscle sirtuin-1 (SirT1), a lysine deacetylase, against maladaptive aortic remodeling associated with chronic oxidative stress and aberrant activation of matrix metalloproteinases (MMPs).

Methods.—In this study, we investigated whether redox dysregulation of SirT1 contributed to the pathogenesis of TAA using fibrillin-1 hypomorphic mice (Fbn1^{mgR/mgR}), an established model of MFS prone to aortic dissection/rupture.

Results: Oxidative stress markers 3-nitrotyrosine and 4-hydroxynonenal were significantly elevated in aortas of MFS patients. Moreover, reversible oxidative post-translational modifications (rOPTM) of protein cysteines, particularly S-glutathionylation, were dramatically increased in aortas of Fbn1^{mgR/mgR} mice, prior to induction of severe oxidative stress markers. Fbn1^{mgR/mgR} aortas and smooth muscle cells (VSMCs) exhibited an increase in rOPTM of SirT1, coinciding with upregulation of acetylated proteins, an index of decreased SirT1 activity, and increased MMP2/9 activity. Mechanistically, we demonstrated that transforming growth factor beta (TGFβ)

#Address correspondence to: Francesca Seta, PhD or Jingyan Han, PhD, Boston University School of Medicine, Department of Medicine, Vascular Biology Section, 650 Albany Street, X720, Boston MA 02118, Tel: (+1) 613-358-7814 setaf@bu.edu or jingyanh@bu.edu.

*these authors contributed equally

AUTHORS CONTRIBUTIONS

BE, SS, YT, LX and YH performed experiments and reviewed the manuscript; JBG analyzed MMP in situ activity images; YW and XY genotyped mice and performed immunostainings; XW analyzed RNA sequencing datasets; PMS measured elastin breaks and aortic diameters; VC provided constructive critique to the manuscript, JH and FS contributed to study design, coordinated the study, designed experiments, analyzed, and interpreted the data, and wrote the manuscript.

DISCLOSURES.

The authors have no conflicts of interest to report.

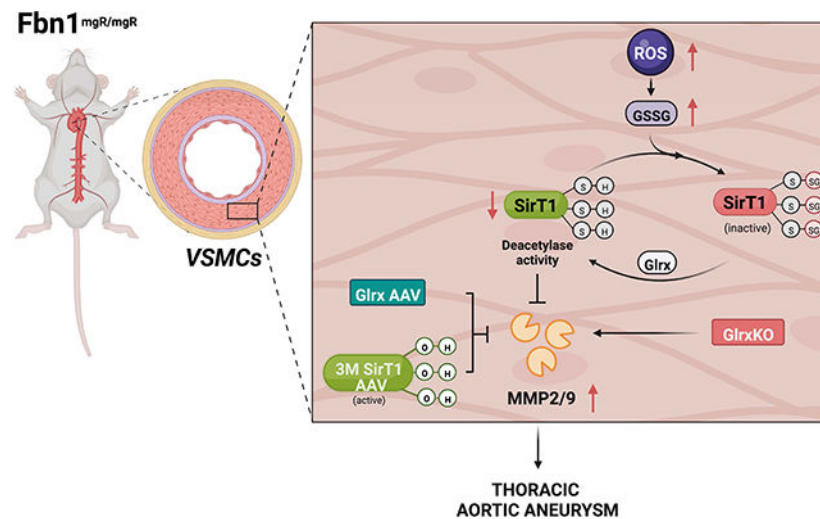
SUPPLEMENTAL MATERIAL.

- Supplemental Figures S1–S13 and legends
- Major Resources Table

that was increased in $Fbn1^{mgR/mgR}$ aortas, stimulated rOPTM of SirT1, decreasing its deacetylase activity in VSMCs. VSMC-specific deletion of SirT1 in $Fbn1^{mgR/mgR}$ (SMKO- $Fbn1^{mgR/mgR}$) mice caused a dramatic increase in aortic MMP2 expression and worsened TAA progression leading to aortic rupture in 50% of SMKO- $Fbn1^{mgR/mgR}$ mice, compared to 25% of $Fbn1^{mgR/mgR}$ mice. rOPTM of SirT1, rOPTM-mediated inhibition of SirT1 activity, and increased MMP2/9 activity, were all exacerbated by deletion of glutaredoxin-1 (Glx), a specific de-glutathionylation enzyme, while being corrected by overexpression of Glrx or of an oxidation-resistant SirT1 mutant in VSMCs.

Conclusions: Our novel findings strongly suggest a causal role of *S*-glutathionylation of SirT1 in the pathogenesis of TAA. Prevention or reversal of SirT1 rOPTM may be a novel therapeutic strategy to prevent TAA and/or TAA dissection/ruptures in individuals with MFS, for which, thus far, no targeted therapy has been developed.

Graphical Abstract



Keywords

aortic aneurysm; Marfan syndrome; *S*-glutathionylation; sirtuin-1; oxidative post-translational modifications

INTRODUCTION

Aortic aneurysms (AA) are abnormal dilatations of the aorta to >150% of its initial diameter, which can become potentially lethal if the aortic wall dissects or suddenly ruptures. AA are broadly classified by anatomical location as thoracic (TAA) or abdominal (AAA), or by etiology as syndromic or non-syndromic. Despite tremendous advances in our understanding of the molecular and genetic mechanisms of AA, there are currently limited therapies for this cluster of vascular conditions. Limited treatment options include blood pressure control and surgical repair, which remains associated with elevated risk of morbidity and mortality¹. Identification of novel therapeutic targets for these potentially lethal vascular diseases is paramount.

AA associated with Marfan syndrome (MFS) are one of the most common syndromic forms of TAA, affecting 1 in 10,000 Americans. MFS is an autosomal dominant genetic disorder linked to mutations in the fibrillin-1 gene (*FBNI*), which encodes a glycoprotein found in extracellular matrix elastin microfibrils. TAA and aortic dissections or ruptures are the most prevalent cardiovascular manifestations of MFS. However, effective therapies to prevent TAA are lacking. As such, there is an urgent need to identify novel molecular mechanisms that can be targeted therapeutically to prevent TAA and its rupture/dissection in patients with MFS. Recent studies have shown that oxidative stress resulting from impaired glutathione system, mitochondrial dysfunction, or the oxidant-generating enzyme NOX4, is increased in aneurysmal aortas of patients with MFS and in animal models²⁻⁴. However, the redox mechanisms by which oxidative stress may cause TAA in MFS are unknown.

Oxidative stress is an imbalance between oxidant production and cellular antioxidant buffer capacity, leading to excessive production of reactive oxygen species (ROS) beyond levels required for homeostatic cellular functions⁵. It has been increasingly appreciated that ROS act as signaling molecules through reversible oxidation of target proteins, thereby regulating their conformation and activity. These reversible modifications, such as oxidation to sulfenic acid, *S*-glutathionylation, and *S*-nitrosylation, mainly occur on cysteine residues, which represent a redox switch to turn on/off redox signaling⁶. Although reversible oxidative post-translational modifications (rOPTM) are strongly associated with oxidative stress in cardiovascular diseases (e.g., atherosclerosis, hypertension, cardiac ischemia), their role in the pathogenesis of oxidative stress-mediated cardiovascular diseases remains unclear⁷. Specifically, the role of rOPTM-mediated redox signaling in TAA in MFS has not been characterized.

Sirtuin-1 (SirT1; mammalian homolog of silent information regulator (Sir2) in yeast) is a nicotinamide adenine dinucleotide (NAD⁺)-dependent deacetylase associated with protective effects in response to metabolic, inflammatory, and oxidative stresses⁸. Lack of SirT1 in the vasculature exacerbates pathological vascular remodeling⁹⁻¹¹. In addition, vascular smooth muscle (VSM) SirT1 deletion was associated with worsening of AAA in aged mice, whereas overexpression of VSM SirT1 prevented AAA in a CaCl₂ periaortic application model¹². Our own studies previously showed that VSM SirT1 is essential for prevention of aortic dissections in mice¹³. This preventive effect occurred through inhibition of oxidant production and reduced activity of extracellular matrix-degrading enzymes matrix metalloproteinases (MMP2 and MMP9)¹³. As MMP2/9 activation is a hallmark of aortic wall remodeling leading to aneurysms and dissections [14], in the present study we examined the role of thiol oxidative stress in redox dysregulation of SirT1 function and consequent hyperactivation of MMPs in TAA development in MFS, using a mouse model of MFS (*Fbn1*^{mgR/mgR} mice), which has been shown to closely mimic the human pathology.

MATERIALS & METHODS.

Data and supporting material are available to the research community upon reasonable request.

Experimental animals.

All experimental procedures were approved by the institutional animal care and use committee (IACUC) at Boston University School of Medicine. Homozygous fibrillin-1 hypomorphic mice (*Fbn1*^{mgR/mgR} mutant mice) were obtained from Dr. Francesco Ramirez under an MTA agreement with Icahn School of Medicine at Mount Sinai, New York, NY, USA and backcrossed into the C57Bl/6J genetic background for >10 generations. Mice were generated by breeding heterozygous *Fbn1*^{mgR/+} mice, which do not develop AA. *Fbn1*^{+/+} (wild type, WT), *Fbn1*^{mgR/+} and *Fbn1*^{mgR/mgR} were produced at expected Mendelian ratios. Genotype was determined at weaning (28-day-old mice) and confirmed at the end of the study using standard end-point PCR on DNA from biopsied tails. Male and female *Fbn1*^{mgR/mgR} mice, and WT littermate controls, were used within 5 months of age, when they had overt TAA but without aortic dissection/ruptures¹⁴. Mice were housed up to four per cage in temperature and humidity-controlled rooms, with a 12-hour light/dark cycle. The mice were fed a standard laboratory diet (PicoLab Verified – 75IF, 5V75, LabDiet, ScottPharma) and water *ad libitum*. Mouse characteristics are summarized in Table 1. In this study, 90% of *Fbn1*^{mgR/mgR} mice (n=50) developed TAA or aortic enlargements within 5 months of age compared with 0% of WT mice (n=40), as expected for this strain, although TAA disease progressed slower than previously reported^{14–16}.

To study the role of vascular smooth muscle (VSM) SirT1 in MFS, we bred *Fbn1*^{mgR/mgR} mice with transgenic mice containing a floxed *SirT1* (*SirT1*^{ex4/ex4}, obtained from Dr. David Sinclair, Harvard Medical School, Boston, MA, USA), and a Cre-recombinase construct driven by the smooth muscle myosin heavy chain 11 (*Smmhc* or *Myh11*) promoter linked to a modified estrogen receptor construct (*Smmhc*^{CreERT2}, stock number 019079, The Jackson Laboratory), which allowed for tamoxifen-inducible removal of *SirT1* in VSM of *Fbn1*^{mgR/mgR} mice. Four-week (wk) old *Smmhc*^{CreERT2}/*SirT1*^{ex4/ex4}/*Fbn1*^{mgR/mgR} mice received tamoxifen (2mg/d) or vehicle for 5 days to obtain VSM-specific *SirT1*-deficient *Fbn1*^{mgR/mgR} mice (SMKO-*Fbn1*^{mgR/mgR}) and *Fbn1*^{mgR/mgR} littermate controls, respectively. In addition, *Glrx1*-deficient (*Glrx*KO) mice, originally generated by Dr. Y.S. Ho (Wayne State University, Detroit, MI, USA)¹⁷ were obtained from Dr. Janssen-Heininger (University of Vermont, VT, USA) and backcrossed into the C57Bl/6J background. Eight-week-old mice were sacrificed to isolate smooth muscle cells, as described below.

Bioinformatic analysis of a single cell RNA sequencing dataset.

Single-cell expression matrices for aneurysmal aortas of mice with a *fibrillin-1* point mutation (*Fbn1*^{Cys1041Gly/+}) and healthy WT controls (24 weeks of age) were obtained from the publicly available Gene Expression Omnibus database (GEO: GSE153534)¹⁸, and were analyzed using Seurat package in R language. Using the predetermined resolution scale described in the original study¹⁸, clusters of two subpopulations of vascular smooth muscle cells (SMC and modulated SMCs (modSMCs)), in WT and *Fbn1*^{Cys1041Gly/+} mice, were isolated for further analysis. Differential expression analysis of all cells within those clusters were performed using the nonparametric Wilcoxon rank-sum test with default parameters ($\log_2FC > 0.20$, FDR-corrected $p < 0.05$). Identified differentially expressed genes (DEGs) were subjected to gene ontology (GO) enrichment analysis to determine whether biological

processes of interest, including oxidative stress, protein acetylation, TGF β signaling, and extracellular matrix remodeling, were significantly altered in the SMC and modSMC from Fbn1^{Cys1041Gly/+} aortas using clusterprofiler and GOplot R packages ¹⁹.

Aortic diameter measurements.

The thoracic aorta of WT and Fbn1^{mgR/mgR} mice was visualized in a parasternal long axis view with high-resolution Doppler ultrasound echocardiography (VEVO3100, VisualSonics Fujifilm, transducer MS550D), using the left subclavian artery as anatomical reference. The diameter of the widest point in the aortic root, ascending aorta or aortic arch segment, which are the locations of TAA development in Fbn1^{mgR/mgR} mice, was measured manually on respiration-gated EKV images acquired at a resolution of 1000Hz frame rate, in the systolic phase of the cardiac cycle, using the linear measurement tool in the VevoLab software (v 7.2). Aortic diameter measurements were confirmed at necropsy. Briefly, mice were humanely euthanized by isoflurane overdose. Whole aortas were gently dissected and imaged in bright field using an Olympus DP25 camera. Aortic diameters, defined as the edge-to-edge widest distance of the ascending aorta or aortic arch, were measured manually in digital images using Image J software, by an investigator blinded to mouse genotype. Aortas were then fresh-frozen in liquid nitrogen or cut into the ascending aorta, the aortic arch, the descending and abdominal aortic segments, which were then embedded into OCT compound. Samples were kept at -80°C until cryo-sectioning and immunostaining, or Western blot.

Reactive oxygen species (ROS) measurement.

Thoracic aorta cryosections (10 μm) from WT (n=10) and Fbn1^{mgR/mgR} (n=10) mice were incubated with 50 μM dihydroethidium solution (DHE, D7008-10MG, Sigma-Aldrich) at 37 $^{\circ}\text{C}$ for 45 min, as we previously described ¹³. DHE is the reduced form of the DNA-binding dye ethidium bromide and is widely used as a fluorescent probe for the detection of ROS, particularly superoxide anion. DHE-stained sections were imaged within 2 h using a Nikon Eclipse 80i epifluorescent microscope and an oil-based 40 \times objective (Boston University Cell Imaging Core). DHE oxidation-derived fluorescent signal, indicative of ROS levels, was quantified using Image J with the thresholding function set at 6.15 pixel/micron. Pixels intensity for each image was then normalized by aortic wall thickness for each aorta.

Elastin fragmentation measurement.

During imaging of DHE-stained aortas, we also acquired images of elastic laminae autofluorescence at 488 nm on the aortic sections. Elastic laminae breaks were identified as dark discontinuous segments in individual fluorescently green elastin lamellae and were manually counted using Image J and normalized to aortic wall area. Three randomly selected aortic regions were analyzed and averaged for each mouse, before expressing data by genotype group. Elastin lamellae were also visualized by staining aortic cryosections with a modified Verhoeff-Van Gieson staining (Elastin Stain kit HT25A, Sigma-Aldrich), as we previously described ¹³. In this case, elastin breaks were counted as discontinuous segments within individual dark brown elastin lamellae.

Vascular smooth muscle cell culture.

Aortic smooth muscle cells were isolated from 8-week-old WT, Fbn1^{mgR/mgR}, or GlrxKO mice, as we previously described¹³. Dissected aortas were incubated with 2 mg/mL collagenase in DMEM at 37 °C for 10 min. Following removal of the adventitia, the endothelial layer was removed by gently rubbing the vessel lumen, and the remaining smooth muscle was then incubated in DMEM supplemented with 2 mg/mL collagenase and 1 mg/mL elastase at 37 °C for an additional 30 min. After dispersing the cell suspension and washing once with PBS, the cells were seeded in collagen-coated 35 mm dishes and allowed to attach for 3 days. VSMCs were sub-cultured in standard 100 mm culture dishes (FalconTM 353002, Fisher Scientific) with DMEM containing 1 g/L glucose, 10% fetal bovine serum FBS (S11150, R&D Systems), and 1% antibiotic-antimycotic solution (15240062, 100x, GibcoTM). VSMCs were used for experiments no later than passage 6. VSMC identity and contractile phenotype were periodically assessed by immunohistochemical staining and Western blot of VSMC contractile proteins. Specifically, VSMCs were confirmed to be > 95% positive for VSM-specific marker calponin1 by immunostaining (17819S, CST, 0.12 µg/mL) (Fig. S1A) and by Western Blot (17819S, CST, 12 ng/mL) (Fig. S1B), up to passage 6. In subsets of experiments, VSMCs were made quiescent in FBS-free DMEM medium for 24 h, then treated with 100 µM H₂O₂ (Sigma-Aldrich) or 20 ng/mL TGFβ1 (Peprotech) for additional 15 min or 24 h, respectively. Thereafter, the cell medium was collected for in-gel zymography analysis, and cell homogenates were prepared in NP-40 lysis buffer, as described below. Replicate experiments with VSMCs were biological replicates on cells prepared from different mice, as indicated in figure legends.

Primary human aortic smooth muscle cells (HASMCs) were purchased from commercial vendors (FC0015, LifeLine Cell Technology and PCS-100-12, ATCC). HASMCs were seeded in standard 100 mm culture dishes in VasuLife LM0002 culture medium supplemented with VasuLife SMC LifeFactors[®] Kit, LS1040 (LifeLine Cell Technology), and used no later than passage 4. To ensure biological replication, replicate experiments were conducted with HASMCs from four different donors: (A) 29-year old African American male, (B) 17-year old Asian male, (C) 23-year old African American female, and (D) 34-year old Caucasian male.

HASMCs or mouse VSMCs were made quiescent in FBS-free medium for 24 h before treatment with TGFβ1 (20 ng/mL, overnight) and H₂O₂ (100 µM, 15 min), with or without the SirT1 activator resveratrol (10µM, 2 hrs), 3M SirT1 AAV (1.3×10¹⁰ vg) or left untreated (control). At the end of the treatment period, cells were collected in RIPA buffer for Western Blot analysis.

Biotin switch assay was performed to detect reversible oxidation of protein cysteines, as we previously described²⁰. Aortas and VSMCs were homogenized in 300 µL of degassed NP-40 lysis buffer (1% NP-40, 150 nM NaCl, 20 mM Tris Base, 2 mM EDTA, 10% glycerol, pH=7.5) supplemented with protease inhibitors (P8340, Sigma-Aldrich), trichostatin A (89730, Cayman Chemical) and 100 mM N-ethylmaleimide (129585, Sigma-Aldrich). Samples were incubated for 1 h at room temperature, then desalted using ZebaTM Spin desalting columns (7K MWCO, 89883, Thermo Fisher Scientific). Total protein

concentration in the eluate was measured using the BCA assay (23225, Pierce™ BCA Protein Assay Kit, Thermo Fisher Scientific). Tris(2-carboxyethyl) phosphine (TCEP, 5mM) (20491, Thermo Fisher Scientific) were added to 50 µg of protein in a total volume of 300 µL, then mixed by rotation for 30 min at room temperature. We then added 3 µL of 250 mM biotin labeling reagent EZ-Link™-Iodoacetyl-PEG-Biotin (21334, Thermo Fisher Scientific), dissolved in anhydrous methyl sulfoxide. The solution was mixed by rotation for 1 h at room temperature. The samples were then incubated with 5 µL of streptavidin magnetic beads (S1420S, New England BioLabs) overnight, under gentle rotation at 4 °C. Beads were collected with a magnet, washed 3× with lysis buffer, then resuspended in 15 µL of NP-40 lysis buffer and 15 µL of reducing Laemmli buffer (2×), and boiled for 5 min at 95 °C to release biotin-labeled proteins for Western blot analysis.

Western blot analysis.

Aortas were placed in a glass-glass grinder (Kontes) with 200 µL of RIPA buffer (9806, CST) freshly supplemented with protease inhibitors and trichostatin A, and manually homogenized on ice. VSMCs were collected in RIPA buffer and homogenized on ice. After 1 h, homogenates were centrifuged at 13,000 rpm at 4 °C for 15 min to collect the supernatants. Protein concentration was measured using the BCA assay (23225, Pierce™ BCA Protein Assay Kit, Thermo Fisher Scientific). Equal amounts of protein (25 µg) were separated by SDS-PAGE in NuPAGE 4–12% Bis-Tris gels (NP0335PK2, Invitrogen) or 4–12% Criterion™ XT Bis-Tris (3415023/3415024, Bio-Rad Laboratories, Inc.), then transferred to 0.45-µm pore PVDF membranes. The membranes were incubated overnight at 4 °C with the following primary antibodies: acetylated H3 (Lys9) (9649, CST, 41 ng/mL), acetylated p53 (Lys 382) (2570S, CST, 0.16 µg/mL), β-actin (4970S, CST, 61 ng/mL), biotin (7075S, CST, 33 ng/mL), GAPDH (2118, CST, 8.4 ng/mL), Glrx1 (ab45953, Abcam, 0.5 µg/mL), HA-tag (3724, CST, 67 µg/mL), 4-hydroxynonenal (ab46545, Abcam, 2 µg/mL), 3-nitrotyrosine (06–284, Millipore, 2 ng/mL), pSmad2 (18338, CST, 58 ng/mL), SirT1 (ab110304, Abcam, 1 µg/mL) or TGFβ1 (A2124, Abclonal, 4.2 µg/mL). The following day, the membranes were washed 3× with TBS-T (sc-24953, Santa Cruz Biotechnology) for 10 min each, then incubated with appropriate HRP-linked secondary antibodies (R1005 or R1006, Kindle Biosciences, LLC, 3.2 µg/mL) for 1 h at room temperature. The membranes were then washed 3× (10 min each) with TBS-T and exposed to the chemiluminescent substrate ECL (R1002, Kindle Biosciences, LLC) to visualize protein bands. Images were acquired using an Image Quant LAS-4000 (General Electric Healthcare Lifesciences, Pittsburgh, PA, USA) with automatic exposure settings. Protein band intensities were analyzed using Image J software (NIH, USA) and normalized to β-actin or GAPDH, which were used as loading controls. Band intensities from the same experimental group were averaged and the data were expressed, in arbitrary units, as fold change of controls, for each replicate Western blot.

Gluthathionylated proteins in VSMCs and aortas were measured by Western Blot using similar procedures except N-ethylmaleimide (10 mM) was added to cell or aortic homogenates to alkylate the free cysteinyl thiol groups in proteins. The cleared tissue lysates were subjected to Western blot analysis in absence of reducing agents and with anti-GSH antibody (101-A-250, Virogen, 2 µg/mL).

Immunofluorescence staining of aortic sections.

Cryo-sections of the ascending aorta (10 μ m) from WT and Fbn1^{mgR/mgR} mice were immunostained for glutathionylated proteins as we previously described²¹. Briefly, the cryo-sections were fixed in cold acetone for 10 min. After air drying, the sections were incubated with 10 mM N-ethylmaleimide for 10 min to alkylate free protein thiols, then blocked with Mouse-On-Mouse reagent (MKB-2213, Vector Laboratories) and 2% BSA/5% goat serum in PBS at room temperature for 1 h each. The sections were then incubated overnight at 4 °C with anti-glutathione antibody (101-A-100, Virogen, 10 μ g/mL) or mouse IgG (I-2000, Vector Laboratories) in 2% BSA/0.025% sodium azide (7144.8-16, Ricca Chemical Company) in TBS. The sections were then developed with anti-mouse Alexa594-conjugated antibody (A11005, Invitrogen, 0.2 μ g/mL) for 1 h at room temperature and mounted using ProLong mounting medium with DAPI (P36981, Invitrogen). For MMP2 immunostaining, aortic sections were incubated overnight at 4 °C with an anti-MMP2 antibody (ab181286, Abcam, 10 μ g/mL) or rabbit IgG (10 μ g/mL), and developed with anti-rabbit Alexa594-conjugated antibody (A11037, Invitrogen, 0.2 μ g/mL) for 1 h at room temperature. Stained sections were imaged and analyzed as described above.

Immunohistochemical staining of human aortas for oxidative stress markers.

Human aortas of donors with Marfan syndrome (2F and 2M, 43–45 years old) were obtained from the Aortic Valve Operative Outcomes in Marfan Patients study (AVOMP), under an MTA with the University of Texas Health Science Center, Houston. Aortas from healthy donors (1M and 3F, 26–57 years old) were obtained from Dr. Katherine Zhang, Boston University through the National Disease Research Interchange (NDRI) repository. All procedures with unidentified human aortas are considered not human subject research and were approved by the Boston University Medical Campus Institutional Review Panel (IRB protocol number H-41011). Upon collection, aortas were immersed in formalin then embedded in paraffin. Paraffin blocks were used to prepare 10 μ m sections. Aortic sections were deparaffinized in xylene, rehydrated in ethanol gradients and stained with hematoxylin & eosin (12013, Newcomer Supply) and elastin (Elastin Stain kit HT25, Sigma-Aldrich), following the manufacturer's recommendations. For the detection of 2-nitrotyrosine, 4-hydroxy-2-nonenal and MMP2, aortic sections were heated for 20 min in an antigen retrieval solution (10mM sodium citrate, pH=6.0) and permeabilized with 0.025% Triton in TBS for 15 min. After incubation with a blocking solution (3% BSA/10% goat serum in TBS) for 1 h, sections were incubated overnight with primary antibodies for 3-nitrotyrosine (06–284, Millipore, 10 μ g/mL), 4-hydroxy-2-nonenal (ab46545, Abcam, 10 μ g/mL) or MMP2 (ab181286, Abcam, 10 μ g/mL). After washing with TBS (3 \times), aortic sections were incubated with biotin-conjugated secondary antibody for 1 h and with Vectastain ABC-HRP reagents for 1 h (PK-4000, Vector Laboratories), before detection with 3,3'-diaminobenzidine (DAB) reagent (SK-4100, Vector Laboratories).

Matrix metalloproteinase (MMP) in situ activity assay.

Thoracic aorta cryo-sections (10 μ m) from WT (n=6) and Fbn1^{mgR/mgR} (n=7) mice were incubated for 1 h at 37 °C with 20 μ L of MMP Red substrate, a proprietary peptide MMP substrate that fluoresces at 590 nm upon cleavage by MMP (13511, Amplitude™

Universal Fluorimetric MMP Activity Assay Kit, AAT Bioquest Inc.), as per manufacturer's recommendations. Stained sections were imaged and analyzed as described above.

Determination of MMP activity using in-gel zymography.

VSMCs from WT and Fbn1^{mgR/mgR} mice were cultured in DMEM with 10% FBS, then made quiescent in FBS-free DMEM for 24 h prior to treatments. Culture medium was collected and concentrated 14× using Amicon[®] Ultra-15 centrifugal filter units (C7715, Sigma-Aldrich). Aortic rings from WT (n=6) and Fbn1^{mgR/mgR} (n=6) mice were incubated in 80 μL of FBS-free DMEM overnight at 37 °C. Culture medium corresponding to 6 μg of VSMC proteins or 40 μL for the aorta medium, respectively, was loaded onto 10% gelatin Novex[™] 10% Zymogram Plus (Gelatin) gels (ZY00100BOX, Invitrogen). Proteins were separated by SDS-PAGE for 3.5 h at 90 V. Human recombinant MMP2 (10 ng) (420-02, PeproTech) was used as an external reference to account for inter-experiment variability. Following protein separation, gels were thoroughly washed 3× with ultrapure water and incubated with Novex[™] Zymogram Renaturing buffer (LC2670, Invitrogen) for 30 min with gentle agitation. Gelatinase activation was performed by incubating the gel in Novex[™] Zymogram Developing buffer (LC2671, Invitrogen), pH 7.4, at room temperature, for 30 min with gentle agitation followed by incubation for 20 h in the dark, at 37 °C, in freshly prepared developing buffer. Gels were stained in a solution containing 0.5% Coomassie Brilliant Blue R-250 (1610400, Bio-Rad Laboratories, Inc.), 40% methanol (v/v), and 10% acetic acid (v/v) for 30 min at room temperature, then de-stained for 1 h in a solution containing 40% methanol (v/v) and 10% acetic acid (v/v). Gel images were acquired using an iBright[™] FL500 imager (ThermoFisher). White band intensities against a dark background, indicative of gelatinase enzymatic activity, mainly pro-MMP9, MMP9, pro-MMP2 and MMP2, were quantified using Image J and expressed as fold change of reference standard (10 ng MMP2) and pg of gelatinase activity per μg protein for cells, or per μL of culture medium for aortas.

Generation of adeno-associated virus (AAV) expressing redox-resistant SirT1 and Glrx.

We designed a DNA plasmid (pcDNA3.1_FLAG_HA_Sirtuin1_3M) expressing a triple mutant form of SirT1 (3M SirT1) in which three cysteine residues were mutated into serine, as we previously described²⁰. We first generated plasmids expressing wild type and a double mutant SirT1 by transforming NEB[®] 5-alpha competent *E. coli* cells (C2987H/C2987I New England Biolabs), using a 5-min transformation protocol provided by the manufacturer. To generate 3M SirT1, we used the double mutant construct (pcDNA3.1_FLAG_HA_Sirtuin1_2M) as a template and inserted the third point mutation (TGT to AGT) using site-directed mutagenesis (SDM), followed by an inverse PCR reaction. For Glrx overexpression, we inserted a FLAG- and HA-tagged Glrx gene sequence downstream of a CMV promoter in an adeno-associated virus (AAV)-MCS plasmid (AF396260, Stratagene). The AAV plasmid with CMV promoter, but without the target gene, was used to generate control AAV. Concentrations of DNA were determined using a NanoDrop[®] ND-1000 UV-Vis spectrophotometer. Correct insertion of the target gene was confirmed by Sanger sequencing.

AAVs overexpressing WT SirT1, 3M SirT1, Glrx and control AAV, containing the AAV2 serotype expression vector, were produced as previously described by Kimura et al. ²². Briefly, HEK293T cells grown in T175 flasks to 70% confluence in DMEM culture medium supplemented with 5% FBS and 4.5 g/L D-glucose were triple transfected at a 1:1:1 molar ratio normalized to plasmid size using Lipofectamine[®]3000 (L3000001, ThermoFisher Scientific) with the following plasmids: (1) AAV plasmid containing AAV replication (Rep) and capsid (Cap) genes (pAAV-DJ/Rep-Cap, VPK-420-DJ, Cell Biolabs); (2) helper plasmid (pHelper); and (3) pAAV expression vector encoding WT SirT1 or 3M SirT1 (synthesized by Quintara Biosciences, Cambridge, MA), Glrx or control. Growth medium was replaced with production medium consisting of 1 g/L D-glucose DMEM supplemented with 1% FBS, 1× GlutaMAX[®] (C35050-061, Thermo Fisher Scientific), 1% penicillin-streptomycin, 10 mM HEPES and 0.075% sodium bicarbonate. On day 3 post-transfection, medium containing the first AAV production was collected and precipitated using a 5× polyethylene glycol (PEG)/NaCl solution (40% PEG 8000 (w/v), 2.5 M NaCl). Medium was replaced with fresh production medium. On day 5 post-transfection, HEK293T cells were collected with 0.5 M EDTA and centrifuged at $750 \times g$ at 4 °C for 15 min. AAV-containing supernatants and culture medium were precipitated with 5× PEG/NaCl solution. Then, AAV suspensions were collected by centrifugation and the virus DNA was extracted by adding an equal volume of chloroform (1:1 v/v). Viral titers were determined using qRT-PCR with primers binding the AAV2 ITRs sequence (Forward: 5'-GGACCCCTAGTGATGGAGTT-3'; Reverse: 5'-CGGCCTCAGTGAGCGA-3'). Final viral titers, expressed as viral genome copies/ μ L (vg/ μ L), were calculated using CFX Maestro Software (Bio-Rad Laboratories, Inc.). AAV integrity was confirmed by detecting the viral capsid proteins VP1, VP2, and VP3 using silver staining (Fig. S2A). Five or 10 μ L AAV aliquots, containing 6.4 or 13×10^{11} vg copies, respectively, were loaded onto 4–12% bis-Tris gels (NP0335PK2, Invitrogen) and proteins were separated by SDS-PAGE. Protein staining was performed using Pierce[™] Silver Staining for Mass Spectrometry kit (24600, Thermo Fisher Scientific), according to the manufacturer's instructions. Viral capsid proteins were identified according to their molecular weights as VP1 (87 kDa), VP2 (73 kDa) and VP3 (62 kDa).

VSMCs were infected with WT SirT1, 3M SirT1, Glrx, and control AAV at 1.5×10^8 – 9.3×10^{10} vg copies per 60 mm dish. After 48 h of infection, the cells were serum-starved prior to treatments. The cells were then collected and processed for biochemical assays. Successful VSMC infection was confirmed using Western blot (Fig. S2B).

SirT1 activity assay.

To examine the effect of *S*-glutathionylation on SirT1 activity, 750 ng of human recombinant sirtuin-1 (AS-72212, Anaspec) was incubated with 20 mM reduced glutathione (GSH) (G6529, Sigma-Aldrich) and 5 mM oxidized glutathione (GSSG) (151193, MP Biomedicals) for 30 min at 4 °C, as we previously described ²³. Excess GSH and GSSG were removed with Zeba[™] Spin desalting columns before performing the deacetylase enzymatic reaction. Untreated and GSSG/GSH-treated SirT1 were incubated with 300 ng of a custom-made SirT1-specific substrate (acetylated-p53^{lys382} peptide tagged with FLAG (DYKDDDDK), synthesized by Anaspec), for 45 min at 37 °C in a pH 7.4 reaction buffer. The reaction was initiated by adding NAD⁺ (500 μ M), an essential SirT1 deacetylase activity

co-factor. Reaction mixtures were subsequently separated by SDS-PAGE in 16.5% Tricine gels (3450063, Bio-Rad Laboratories, Inc.) under non-reducing conditions. The p53 peptide was transferred to a 0.2- μ m pore PVDF membrane (1620177, Bio-Rad Laboratories, Inc.) using a Trans-Blot Turbo[®] system (1701450, Bio-Rad Laboratories, Inc.) optimized for low molecular weight protein detection (5 min, 1.3 A). Membranes were blocked in TBS-T with 5% dry milk (w/v) for 1 h and incubated overnight at 4 °C, with an anti-acetyl p53 (lys382) antibody (2570S, CST, 0.16 μ g/mL). Membranes were subsequently incubated with an anti-rabbit HRP-linked secondary antibody (R1006, Kindle Biosciences, LLC, 3.2 μ g/mL) for 1 h. Chemiluminescent signals were developed with a digital-ECL substrate (R1002, Kindle Biosciences, LLC) and captured using an iBright[™] FL500 imaging system (Thermo Fisher Scientific). Total p53 was detected by stripping the membrane for 20 min in Restore[™] Western blot stripping buffer (21059, Thermo Fisher Scientific), then re-blotting with an anti-FLAG antibody (2368, CST, 84 ng/mL). The membranes were developed as described for the acetylated p53 fraction. Band intensities were quantified using Image J. SirT1 deacetylase activity was determined by calculating the ratio of acetylated to total p53 peptide band intensities and expressed as acetylated/total p53 per μ g SirT1 per hour.

TGF β activity assay.

To measure bioactive TGF β , we used mink lung epithelial cells (MLEC) harboring a plasminogen activator inhibitor 1 (PAI-1) promoter-luciferase construct, a kind gift from Dr. Matthew Layne, Boston University School of Medicine, as he previously described²⁴. Briefly, MLEC reporter cells were seeded in triplicates at a density of 10,000 cells per well into 96-well plates and incubated for 2 days at 37° C in DMEM with 4.5 g/L glucose, 10% FBS, and 250 μ g/mL G418. Mouse plasma (6.7 μ L), collected from WT (n=23) and Fbn1^{mgR/mgR} (n=21) mice, was then added to 193.3 μ L of FBS-free DMEM in each well, overnight. Cells were then washed with PBS and harvested in lysis buffer for the measurement of luciferase activity, an index of bioactive TGF β , with a luciferase detection kit (Promega), as per manufacturer's recommendations. TGF β levels in plasma samples were extrapolated from a standard curve prepared with MLEC reporter cells treated with increasing amounts of recombinant TGF β 1 (0.1–10 ng/mL) (R&D).

Statistical analysis.

Mouse group sizes were determined by a priori power analysis using *G*Power* software (<http://psycho.uni-duesseldorf.de/abteilungen/aap/gpower3>), based on expected effect size inferred from our previously published studies^{20,21,25}. To limit experimental bias, researchers were kept blinded to mouse genotypes. Upon data acquisition, genotype or treatment groups were unblinded by one investigator (FS), who performed statistical analyses using Graphpad Prism v.9.2 software. Datasets were first subjected to a D'Agostino and Pearson normality test (for experiments with n \geq 8) or the Shapiro-Wilk normality test (for experiments with 4 < n < 8) to determine whether the distributions were Gaussian. Means of normally distributed datasets were compared using Student's t-test. Datasets that did not follow a Gaussian distribution were analyzed using non-parametric tests. Experiment with multiple treatment and genotype groups were analyzed using one- or two-way ANOVA with appropriate post-hoc multiple comparison analysis. Survival rates and incidence of TAA of Fbn1^{mgR/mgR} and SMKO-Fbn1^{mgR/mgR} mice and in male vs female Fbn1^{mgR/mgR} mice

were compared with Log-rank (Mantel-Cox) test. Across-test multiple test correction was not applied. *P* values < 0.05 were considered significant. Data are expressed as the mean ± SEM, therefore representative images for figures were chosen to best represent the mean ± SEM. The number of replicates and statistical tests used in each experiment are indicated in figure legends. For experiments with VSMCs, replicate experiments in figure legends and text indicate individual VSMC preparations from different mice, to ensure biological, rather than technical, replication. These data were reported as fold-change vs WT or control treatment for each replicate experiment before averaging by genotype or treatment group. In all figure graphs, female and male mice used in each experiment or for isolation of VSMCs used for experiments, are indicated with a circle or square symbol, respectively.

RESULTS

Incidence of aortic aneurysm and mortality in *Fbn1^{mgR/mgR}* mice.

We used hypomorphic *Fbn1^{mgR/mgR}* mice, a well-established model of Marfan syndrome^{14–16}. Nineteen of 50 (38%) *Fbn1^{mgR/mgR}* mice were found dead at 2.7±0.2 months of age, because of hemothorax or thoracic hemorrhage due to a rupture in the atrium (9) or ruptured TAA (4), diaphragmatic hernia with inverted organs (1) or unknown causes (5). Among the 62% (31 of 50) surviving *Fbn1^{mgR/mgR}* mice, 90% (28 of 31) developed overt TAA around 4 months of age (4.5±0.2 months), compared to no TAA, aortic enlargements or deaths in WT littermates (0 of 40) (Table 1), as expected for this strain. Aortic diameter measurements in vivo (Fig. S3A) and morphological analysis at necropsy (Fig. S3B) confirmed increased aortic diameter in *Fbn1^{mgR/mgR}* (n=12) compared with WT mice (n=12) (1.87 ± 0.13 mm vs 1.02 ± 0.02 mm; *p*<0.0001).

We observed substantial sex differences in mortality and TAA development between male and female *Fbn1^{mgR/mgR}* mice. Specifically, 50% (14 of 28) *Fbn1^{mgR/mgR}* males were found dead compared to 23% (5 of 22) *Fbn1^{mgR/mgR}* females (*p*=0.03; Fig. S4A), although average age of death for females was lower than for males (1.6±0.4 months in females vs 3.8±0.4 months in males). Moreover, among the surviving mice, 13 of 14 (93%) male *Fbn1^{mgR/mgR}* mice had overt TAA, whereas 8 of 17 (47%) females had TAA and 6 of 17 (35%) developed aortic enlargements (i.e., aortic diameter was enlarged but <150% than WT), with the majority of TAA occurring within 5 months of age (*p*=0.03; Fig. S4B). Overall, these results suggested that *Fbn1^{mgR/mgR}* males had accelerated or more severe development of the aneurysmal phenotype, compared with females.

S-glutathionylation is increased in *Fbn1^{mgR/mgR}* mouse aortas.

To examine VSM-specific molecular processes involved in the pathogenesis of TAA in MFS, we conducted an unbiased bioinformatic analysis on the only publicly available single cell RNA sequencing dataset (GSE153534) from aortas of a mouse model of MFS (*Fbn1^{C1041G/+}* mice)¹⁷. Despite the fact that *Fbn1^{C1041G/+}* mice are known to have a less severe vascular phenotype than *Fbn1^{mgR/mgR}* mice, this analysis provided valuable insights into potential common molecular signatures and pathways in VSM cell populations that may contribute to the pathogenesis of TAA. Differentially expressed gene sets identified in WT smooth muscle cells (WT-SMC) and two distinct subpopulations of

Fbn1^{C1041G/+} smooth muscle cells (MFS-SMC and MFS-modSMC) were subjected to gene ontology (GO) enrichment analysis to identify biological pathways significantly altered in MFS VSMCs. Among key biological processes, “Response to oxidative stress”, “Protein acetylation”, “TGF receptor signaling pathway”, and “Extracellular matrix reorganization” were significantly enriched in *Fbn1*^{C1041G/+} VSMCs (Fig. S5A). Notably, the significance of enrichment of these pathways was greatly enhanced in the modified SMC cluster of *Fbn1*^{C1041G/+} VSMCs (MFS-modSMC), a distinct subpopulation of VSMCs with an MFS disease-specific signature characterized by trans-differentiation toward a fibroblast-like phenotype and extracellular matrix remodeling, as reflected by $-\log_{10}(p \text{ adjusted})$ value (Fig. S5B). These results suggested involvement of redox signaling, protein acetylation, and TGF β signaling in the pathogenesis of aortic wall remodeling in MFS.

Consistent with these bioinformatic findings, levels of 3-nitrotyrosine (3-NT) and 4-hydroxynonenal (4-HNE), two major indicators of free radical-induced oxidation of proteins and lipids, were significantly increased by 157 ± 54 - ($p=0.04$) and 88 ± 44 -fold ($p=0.05$), respectively, in aortic sections of individuals with MFS ($n=3$), compared to those in healthy donors ($n=3$) (Fig. 1A). Similarly, levels of ROS were significantly increased in aortas from *Fbn1*^{mgR/mgR} mice compared to those in WT mice, as indicated by increased red fluorescent signal on DHE-stained aortic sections (836 ± 70 AU in WT, $n=10$ vs 1209 ± 142 AU in *Fbn1*^{mgR/mgR}, $n=10$; $p=0.03$; Fig. 1B).

Consistent with increased oxidants, we found increased total reversible oxidative post-translational modifications of proteins (rOPTM), as determined using a biotin switch assay (2.3 ± 0.6 -fold increase in *Fbn1*^{mgR/mgR} mice ($n=5$) compared to WT mice ($n=5$); $p=0.008$) (Fig. 2A). S-glutathionylation is a major form of rOPTM, by which glutathione binds to cysteine residues as a result of increased levels of intracellular oxidants or reduction in de-glutathionylation enzymes, such as glutaredoxins^{25–27}. We found that S-glutathionylation (Pr-SSG) was induced in the aortas of *Fbn1*^{mgR/mgR} mice, assessed using Western blot (0.9 ± 0.1 AU in WT, $n=6$ vs 1.6 ± 0.1 AU in *Fbn1*^{mgR/mgR}, $n=5$; $p=0.02$) (Fig. 2B). Increased Pr-SSG in aortas of *Fbn1*^{mgR/mgR} mice were observed as early as 2 months of age, in both thoracic and abdominal aortic regions (Fig. S6). These findings were further corroborated by increased levels of Pr-SSG adducts in *Fbn1*^{mgR/mgR} aortic sections as indicated by the heightened immunoreactive Pr-SSG fluorescent signal (Fig. 2C); the detected Pr-SSG appeared to increase in VSMCs (Fig. 2C). In contrast, levels of 3-NT and 4-HNE, two forms of irreversible oxidative modification, in whole aortic homogenates of 2- or 4-month-old *Fbn1*^{mgR/mgR} mice were not significantly higher compared to WT mice (Fig. 2D and Fig. S6). Taken together, these findings suggest that induction of aortic protein S-glutathionylation and/or other rOPTM is an early oxidative event in aortas of MFS mice, preceding other oxidative modifications, including 3-NT and 4-HNE, two widely accepted oxidative stress markers. As S-glutathionylation is a primary molecular mechanism of redox signal transduction by modulating target protein’s function and stability, our data suggested that it may contribute to TAA pathogenesis via redox dysregulation of key enzymes in VSMCs.

Induction of reversible oxidation on Sirtuin-1 is associated with impaired deacetylase activity in Fbn1^{mgR/mgR} mice.

We previously reported that lack of SirT1 in VSMCs caused aortic dissection/rupture in mice treated with the hypertensive peptide angiotensin II¹³. We also previously showed that S-glutathionylation on redox sensitive cysteine residues nearby SirT1 catalytic site, impairs SirT1 deacetylase activity in hepatic cells, underpinning the pathogenesis of fatty liver disease¹⁹. In this study, we thus examined the changes in SirT1 redox status and deacetylase activity in aortas of Fbn1^{mgR/mgR} mice. As shown in Fig. 3A, rOPTMs of SirT1 were induced in VSMCs from Fbn1^{mgR/mgR} mice compared with that in WT mice (1.0 ± 0.5 AU in WT vs 1.7 ± 0.8 AU in Fbn1^{mgR/mgR}, $n=7$ replicate experiments; $p=0.05$). Moreover, total protein levels of SirT1 were significantly decreased in aortas of Fbn1^{mgR/mgR} mice (1.5 ± 0.1 AU in WT, $n=15$ vs 0.7 ± 0.1 AU in Fbn1^{mgR/mgR}, $n=13$; $p<0.0001$), which was associated with decreased SirT1 activity, indicated by increased acetylated p53^{lys379}, a well-known SirT1 deacetylation target²⁸ (0.3 ± 0.0 AU in WT, $n=4$ vs 0.6 ± 0.1 AU in Fbn1^{mgR/mgR}, $n=5$; $p=0.004$) (Fig. 3B).

To further examine whether decreased SirT1 activity contributed to TAA development in Fbn1^{mgR/mgR} mice, we generated Fbn1^{mgR/mgR} mice with tamoxifen-inducible VSM-specific SirT1 deletion (SMKO-Fbn1^{mgR/mgR}) (Fig. 3C). SMKO-Fbn1^{mgR/mgR} developed very severe TAA (aortic diameter: 1.0 ± 0.0 mm in WT, $n=12$, 1.8 ± 0.1 mm in Fbn1^{mgR/mgR}, $n=12$ and 3.4 ± 0.5 mm in SMKO-Fbn1^{mgR/mgR}, $n=8$; $p=0.0002$ Fbn1^{mgR/mgR} vs SMKO-Fbn1^{mgR/mgR}) (Fig. 3D). Moreover, TAA in SMKO-Fbn1^{mgR/mgR} mice ruptured within 1.4 ± 0.3 months of SirT1 deletion, resulting in 5 of 10 (50%) deaths, compared to 2 of 8 (25%) deaths in Fbn1^{mgR/mgR} mice at 2.9 ± 0.1 months of age ($p=0.01$; Fig. 3E). These findings strongly indicate that SirT1 in VSMCs is required for the maintenance of the aortic wall integrity and lack of its activity dramatically worsens TAA progression and accelerates TAA rupture in MFS mice.

S-glutathionylation inhibits SirT1 activity in Fbn1^{mgR/mgR} VSM cells.

We next examined whether the enhanced S-glutathionylation in MFS mice contributed to SirT1 functional impairment. Firstly, we found that the levels of TGFβ1, a profibrotic cytokine known to be elevated in MFS patients, were elevated in aortas of Fbn1^{mgR/mgR} mice (1.0 ± 0.1 AU in WT, $n=5$ vs 1.9 ± 0.1 AU in Fbn1^{mgR/mgR}, $n=5$; $p=0.0002$, Fig. 4A and Fig. S7 for phosphorylated Smad2, an index of TGFβ bioactivity), albeit no differences in circulating TGFβ were detected between WT and Fbn1^{mgR/mgR} mice (Fig. S8). Treatment of WT VSMCs with TGFβ1 (20 ng/mL) induced a 2.4 ± 0.5 -fold increase in Pr-SSG levels, compared to vehicle ($n=5$ independent cell preparations; $p=0.02$) (Fig. 4B). Secondly, we demonstrated that treating VSMCs with TGFβ1 (20 ng/mL) or oxidant H₂O₂ (100 μM) induced rOPTM of cysteine residues on SirT1, compared with that in control cells, as determined using a biotin switch assay¹⁹ (TGFβ1: 1.0 ± 0.1 AU in vehicle- vs 1.4 ± 0.4 AU in TGFβ1-treated VSMCs, $n=7$ replicate experiments; $p=0.04$; H₂O₂: 1.0 ± 0.4 AU in vehicle- vs 1.9 ± 1.1 AU in H₂O₂-treated VSM cells, $n=8$ replicate experiments; $p=0.04$; respectively) (Fig. 4C). Furthermore, the levels of rOPTM of SirT1 were significantly increased in VSMCs from mice that lacked glutaredoxin-1 (GlxKO), a thioltransferase that selectively reverses S-glutathionylation, compared with cells from WT mice (1.0 ± 0.0

AU in WT vs 1.8 ± 0.3 AU in Glrx-KO, $n=4$ replicate experiments; $p=0.03$) (Fig. 4D). In contrast, overexpression of Glrx significantly decreased ReOx SirT1 in Fbn1^{mgR/mgR} VSMCs by 50%, and increased SirT1 activity (i.e. lower levels of acetylated H3^{lys9}, a well-known SirT1 deacetylation target), compared to those in control cells (Fig. 4E). Taken together, these results indicated that *S*-glutathionylation was the predominant rOPTM on SirT1 and inhibited its activity, in Fbn1^{mgR/mgR} VSMCs.

To test the direct effect of *S*-glutathionylation induction on SirT1 activity, we incubated recombinant human SirT1 with a mixture of reduced and oxidized GSH (GSH:GSSG at 1:3 ratio), which has been shown to induce *S*-glutathionylation via thiol-disulfide bond exchange. GSSG significantly decreased SirT1 deacetylase activity by ~90%, measured using a SirT1 activity assay (acetylated/total p53 per μg SirT1 per hour: 1.9 ± 0.3 in control vs 0.25 ± 0.0 in SirT1 vs 2.1 ± 0.2 in SirT1/GSSG, $n=4$ replicate experiments; $p=0.0004$ control vs SirT1; $p=0.0002$ SirT1 vs SirT1/GSSG) (Fig. 5A). Consistent with *S*-glutathionylation inhibiting SirT1 activity, acetylated p53^{lys379} was significantly increased in GlrxKO VSMCs (1.0 ± 0.1 AU in WT vs 2.2 ± 0.1 AU in GlrxKO, $n=4$ replicate experiments; $p=0.0003$) (Fig. 5B), and in Fbn1^{mgR/mgR} VSMCs (1.0 ± 0.0 AU in WT vs 1.3 ± 0.0 AU in Fbn1^{mgR/mgR}, $n=3$ replicate experiments; $p=0.03$) (Fig. 5C), compared with that in WT cells. Notably, overexpressing an oxidation resistant SirT1 mutant (3M SirT1) with an AAV (Fig. S9), restored SirT1 activity in Fbn1^{mgR/mgR} VSMCs as reflected by lower ac-p53, compared with Fbn1^{mgR/mgR} cells treated with control AAV (ac-p53: 1.0 ± 0.0 AU in Fbn1^{mgR/mgR}/AAV-control, $n=4$ vs 0.7 ± 0.0 AU in Fbn1^{mgR/mgR}/AAV-3M SirT1, $n=4$; $p=0.01$) (Fig. 5D). Interestingly, treatment with resveratrol, a well-characterized activator of SirT1²⁹, was less effective than AAV-3M SirT1 in restoring SirT1 activity in TGF β 1/H₂O₂-treated human (Fig. 5E) and mouse (Fig. S10) VSMCs.

Collectively, these data indicate that (1) SirT1 activity was impaired in Fbn1^{mgR/mgR} VSMCs; (2) *S*-glutathionylation of SirT1 appears to be a redox mechanism responsible for this functional deficit; and (3) preventing SirT1 oxidation is more effective than conventional SirT1 activators, such as resveratrol, in rescuing its impaired de-acetylase activity in the pathological oxidative conditions of MFS.

S-glutathionylated SirT1 is associated with increased MMP activity in Fbn1^{mgR/mgR} mouse aortas and VSMCs.

We previously reported that aortic dissections/ruptures in mice with VSM-specific SirT1 deletion in response to AngII, were associated with increased extracellular matrix-degrading enzyme matrix metalloproteinase MMP2 and MMP9 activity¹³. Based on the novel finding that SirT1 *S*-glutathionylation inhibits its activity in Fbn1^{mgR/mgR} VSMCs, we evaluated the associations among reversibly oxidized SirT1, MMP activation, and TAA development in Fbn1^{mgR/mgR} mice. Upregulation of MMP2 is known to participate in aortic wall remodeling during aortic aneurysm development³⁰, also in Fbn1^{mgR/mgR} mice¹⁵. Consistently, we observed that MMP2 protein levels were significantly increased in aneurysmal sections of aorta from MFS patients, accompanied by severe elastin fragmentation (Fig. 6A). Similarly, MMP2 mRNA levels were dramatically upregulated in the modified SMC from Fbn1^{C1041G/+} aortas compared to those in WT SMC, in the bioinformatic analysis we

performed of a published single cell RNA sequencing dataset (GSE153534)¹⁷ (Fig. S11). More importantly, we found that MMP activity was elevated in the aortic sections of Fbn1^{mgR/mgR} mice as assessed using an MMP *in situ* activity assay (422.8 ± 58.1 AU/wall thickness in WT, n=6 vs 653.7 ± 195.5 AU/wall thickness in Fbn1^{mgR/mgR}, n=7; *p*=0.03, Fig. 6B), which was accompanied by severe elastin laminae fragmentation (0.3 ± 0.2 in WT, n=9 vs 3.6 ± 0.5 in Fbn1^{mgR/mgR}, n=11; *p*<0.0001, Fig. 6B). These findings were corroborated in VSMCs and aortas of Fbn1^{mgR/mgR} mice using in-gel zymography (1.0 ± 0.2- in WT vs 2.6 ± 0.5-fold change pg/μg protein in Fbn1^{mgR/mgR}; n=7 independent cell preparations; *p*=0.01) (Fig 6C and Fig. S12). Moreover, deletion of SirT1 from VSMCs, significantly increased MMP2 expression (Fig. 6D), associated with severe elastin fragmentation (Fig. 3D and Fig. S13), in SMKO-Fbn1^{mgR/mgR} mice, underscoring that VSM SirT1 is crucial to suppress MMP activation in the aortic wall, consistent with our previous report¹³.

We next examined whether the thiol redox dysregulation of SirT1 was causally linked to the hyperactivation of MMPs in MFS. VSMCs isolated from GlrxKO mice, in which SirT1 activity was decreased (Fig. 5B), showed significantly increased MMP activity compared to WT cells (1.0 ± 0.0 in WT vs 2.5 ± 0.3-fold change pg/μg protein in GlrxKO; n=4 independent cell preparations, *p*=0.004) (Fig. 7A). Conversely, overexpression of Glrx with AAV was sufficient to lower MMP activity in Fbn1^{mgR/mgR} VSMCs (168.7 ± 23.2 in Fbn1^{mgR/mgR}/AAV-control, n=4 vs 98.2 ± 14.9 pg/μg protein in Fbn1^{mgR/mgR}/AAV-Glrx, n=4; *p*=0.05) (Fig. 7B). Moreover, overexpression of oxidation resistant SirT1 mutant (3M SirT1) significantly decreased MMP activity in Fbn1^{mgR/mgR} VSMCs (241 ± 19 in Fbn1^{mgR/mgR}/AAV-control vs 169 ± 13 pg/μg protein in Fbn1^{mgR/mgR}/AAV-3M SirT1, n=3; *p*=0.03) (Fig. 7C), compared with controls.

Collectively, these results identified a *S*-glutathionylation-dependent redox mechanism by which impaired SirT1 activity contributed to the pathogenesis of TAA, at least in part, via increased MMP activation in MFS.

DISCUSSION

Aortic aneurysms (AA) are aortic enlargements that can gradually worsen into aortic dissections and ruptures, potentially leading to death. Increased oxidant levels have recently been reported in aneurysmal aortas of patients^{31–33} and in animal models^{4,34,35}. However, the underlying redox molecular mechanisms associated with the development of AA remain unclear. In this study we found that reversible OPTM of SirT1 is a novel redox mechanism underlying SirT1 functional impairment in VSMCs, thereby contributing to the pathogenesis of TAA in Marfan syndrome (MFS). This work could lead to identification of novel therapeutic strategies to prevent TAA and aortic dissection/rupture in MFS.

The major novel findings of this study (summarized in the Graphic Abstract) were that (1) reversible OPTM of proteins, mainly resulting from *S*-glutathionylation, were elevated in aortas and VSMCs of a mouse model of MFS (Fbn1^{mgR/mgR} mice), which develop TAA spontaneously within 5 months of age. (2) SirT1, a redox sensitive protein, was reversibly oxidized in aortas and VSMCs of Fbn1^{mgR/mgR} mice, leading to its impaired deacetylase

activity and aberrant activation of matrix metalloproteinases (MMPs), which is a major culprit of aneurysmal remodeling³⁰. (3) Inhibition of reversible SirT1 OPTM through overexpressing glutaredoxin-1 or an oxidation-resistant SirT1 mutant was able to rescue SirT1 activity and suppress MMP hyper-activity in VSMCs of MFS mice.

S-glutathionylation refers to the formation of glutathione adducts (Pr-SSG) on protein thiolate groups ($P-SH \leftrightarrow P-S^-$) and is the predominant form of rOPTM due to the high relative abundance of intracellular glutathione (GSH) and its stability³⁶. *S*-glutathionylation is tightly regulated by deglutathionylation enzymes, including the thioltransferase glutaredoxin-1 (Glx) and glutathione reductase³⁷. Impairment of the de-glutathionylation system has been implicated in a variety of diseases associated with oxidative stress, including non-alcoholic fatty liver disease, and lung and cardiovascular diseases³⁷. We previously showed that the *S*-glutathionylation status of Rac-1 in endothelial cells was crucial for the maintenance of endothelial permeability in a mouse model of atherosclerosis, and that barrier function was partially restored by overexpressing Glrx²⁰. However, the role of *S*-glutathionylation or other forms of rOPTM in the development of TAA had not been previously studied. This is the first study to show that aortas and VSMCs of *Fbn1*^{mgR/mgR} mice, a well-established model of MFS prone to TAA and ruptures, had increased overall protein *S*-glutathionylation, providing the first evidence for the involvement of redox signaling events in the pathogenesis of TAA. SirT1, a lysine deacetylase that protects the aortic wall from aortic dissections and ruptures¹³, was reversibly oxidized in *Fbn1*^{mgR/mgR} aortas and VSMCs, resulting in decreased SirT1 deacetylase activity in combination with SirT1 downregulation. These findings are further supported by our bioinformatic analysis of a publicly available single cell RNA sequencing dataset obtained from aortas of *Fbn1*^{C1041G/+} mice¹⁷, another fibrillin-1 mutant mouse model of MFS. This analysis showed that “Response to oxidant stress” and “Protein acetylation” were among the most significantly differentially regulated biological processes in VSMCs of thoracic aorta from *Fbn1*^{C1041G/+} mice, especially in a subpopulation of de-differentiated VSMCs, suggesting a new molecular basis of redox dysregulation of protein acetylation in TAA in MFS. In addition, our findings were consistent with clinical reports of increased oxidants in aortas and VSMCs of patients with MFS³, confirmed by our own immunostainings (Fig. 1A–B).

Increased levels of overall protein *S*-glutathionylation and reversible cysteine oxidation on SirT1 in *Fbn1*^{mgR/mgR} mice were mimicked in VSMCs by treatment with transforming growth factor β 1 (TGF β 1), a profibrotic cytokine that has been shown to be upregulated in MFS as a consequence of *fibrillin-1* mutations³⁸. These increases in *S*-glutathionylation indicated that TGF β 1 may be an important driver of pathogenic redox signaling in this mouse model. This is not surprising considering that TGF β is a downstream effector of angiotensin II³⁹ and a transcriptional activator of the hydrogen peroxide-generating enzyme NADPH oxidase (Nox) isoform 4 (Nox4)⁴⁰ in VSMCs. A recent report identified NOX4/Nox4 as the major source of TGF β -mediated ROS production in aortas and VSMCs from patients and animals with MFS⁴. However, inhibition of TGF β activity to prevent TAA in MFS remains controversial^{16,41} as inhibition of TGF β with neutralizing antibodies^{42,43} or using the angiotensin II blocker losartan⁴⁴, yielded contrasting results in animal studies and in the clinic^{45,46}. Interestingly, we found that TGF β levels were increased in the aorta (Fig.

4A), but not in plasma, of MFS mice (Fig. S8), suggesting that locally expressed, i.e aortic, TGF β , possibly during specific phases of disease progression¹⁶, could represent a rational, albeit difficult to achieve, therapeutic target to ameliorate TAA development in MFS, as opposed to constraining circulating TGF β with a neutralizing antibody. In addition, targeting TGF β downstream pathological redox signaling pathways, such as S-glutathionylation of SirT1, could be an additional novel therapeutic strategy for TAA in MFS.

Our study also suggests that restoring thiol redox homeostasis could represent a novel therapeutic approach to prevent TAA in MFS. Elimination of ROS using a non-targeted antioxidant could impair physiological redox signaling cascades necessary for vascular function, and negatively impact adaptive responses to insults and stress, which may be one of the reasons why antioxidant vitamin supplements have repeatedly failed to prevent vascular diseases in clinical trials⁴⁷. Furthermore, since reversible oxidative post-translational modifications (rOPTM) of protein cysteines, which we showed dramatically elevated in MFS mouse aortas, are reversible, they are an attractive therapeutic target. S-glutathionylation is a post-translational modification that represents a major mechanism of oxidative signal transduction and targets multiple proteins containing reactive cysteine thiols, thereby effectively transmitting redox signals to induce cellular responses. The proteins targeted for S-glutathionylation depend on the spatial and temporal distribution of reactive oxygen species (ROS). It is conceivable that in MFS aortas, NOX4 is activated in response to a stimulus, such as locally hyperactive TGF β in specific stages of disease progression, and that the resulting H₂O₂ can induce S-glutathionylation of one or more nearby redox-sensitive target proteins. Glrx subcellular distribution and proximity to target proteins confer a greater specificity on the redox regulation of target proteins, and the signaling cascades that ensue. Although the present study focused on the Glrx/SirT1-SSG/MMP2 redox axis, we believe additional mechanisms underlying the Glrx-dependent regulation of MMP2 may be at play in TAA development in MFS.

SirT1 is a nicotinamide adenine dinucleotide (NAD⁺)-dependent and class III histone deacetylase, and the most well-characterized member of the sirtuin family in mammals⁸. Preserving SirT1 activity in the vasculature has been shown to be essential to support the structural and functional integrity of the arterial wall through modulation of antioxidant, anti-inflammatory, anti-apoptotic and/or anti-senescent pathways in endothelial and smooth muscle cells^{9–11}. Our previous study showed that overexpression of SirT1 in VSM protected mice from obesity-induced arterial stiffening through anti-inflammatory and antioxidant effects⁴⁸. We also showed that lack of SirT1 in VSM-specific SirT1 null mice resulted in increased susceptibility to aortic wall dissections and ruptures¹³. These effects resulted from increased activation of MMP and subsequent elastin degradation¹³. Consistent with our previous findings, in this study, we found that lack of SirT1 in VSM greatly worsens TAA development and incidence of aortic ruptures in Fbn1^{mgR/mgR} mice (Fig. 3C–E). Likewise, Chen et al. showed that lack of VSM SirT1 increased the incidence of abdominal AAA in aged VSM-specific SirT1 null mice, while overexpression of SirT1 in VSM protected against p21-dependent VSM cell senescence associated with AAA development¹². Moreover, activation of SirT1 by caloric restriction⁴⁹ prevented angiotensin II-induced AAA in mice via SirT1-mediated epigenetic regulation of the MMP2 gene promoter⁵⁰. Others showed that administration of resveratrol, a non-specific SirT1

activator, significantly decreased the incidence of TAA in a Fbn1^{C1041G/+} mouse model⁵¹. Collectively, these studies showed that preservation of SirT1 activity in the aortic wall may decrease the incidence of TAA, and potentially other forms of AA, in part by suppressing MMP activity. However, the translational value of these findings has been limited primarily due to poor effectiveness and/or selectivity of SirT1 activators. In our experimental conditions, resveratrol stimulated SirT1 de-acetylase activity only partially in human and mouse VSMCs in response to TGFβ1/H₂O₂ (Fig. 5E), indicating that resveratrol, and possibly other current putative activators, may not be effective in activating the oxidized SirT1 in a highly oxidant milieu that occurs in aneurysmal aortic regions of MFS patients. Therefore, manipulating redox status of SirT1 could be a novel approach to improving its activity in VSMCs and impeding TAA development and/or TAA dissection/rupture in MFS.

We previously showed that *S*-glutathionylated SirT1 exhibited decreased deacetylase activity^{52,53} and promoted lipid accumulation in Glrx null mice, resulting in non-alcoholic fatty liver disease, which was partially reversed by replenishing Glrx activity¹⁹. Importantly, a redox-resistant SirT1 mutant, with intact deacetylase activity, protected against hepatic metabolic and oxidative stress⁵⁴. In the current study, we found that overexpression of Glrx or a redox-resistant SirT1 mutant significantly prevented the activation of MMP in VSMCs of Fbn1^{mgR/mgR} mice, providing the first evidence that these therapeutic strategies may be effective in reducing the incidence of TAA and/or TAA dissection/rupture in individuals with MFS.

Lastly, we observed sex differences in the incidence of TAA and deaths in Fbn1^{mgR/mgR} mice with males experiencing a more severe aneurysmal phenotype than female mice (50% vs 23% mortality). Interestingly, deaths occurred earlier in females (1.6±0.4 months) than in males (3.8±0.5 months) and were caused mainly by rupture in the atrium, even in absence of TAA, suggesting severe cardiac impairment.

Our study presents the following limitations: (1) Our findings on increased aortic rOPTM and reversibly oxidized SirT1 were obtained using the Fbn1^{mgR/mgR} MFS model. Therefore, the results of our study may not be generalizable to other AA models, although oxidative stress, reduced SirT1 activity and increased MMP activity have been shown as contributors to several forms of aortic aneurysm. (2) The time-course of TAA development and progression to dissection/rupture appears to be less severe in our Fbn1^{mgR/mgR} mice than previously reported¹⁴⁻¹⁶, possibly due to a different genetic background of our mice vis-a-vis mice in previous reports. Our study underscores the paramount importance of reporting in detail the time-course of TAA development, genetic background and sex differences in studies with mouse models of Marfan syndrome, particularly when pharmacological or other therapeutic interventions are tested. (3) We did not evaluate whether other forms of protein rOPTM, such as *S*-carbonylation and/or *S*-nitrosylation, were involved in the development of AA. We focused on *S*-glutathionylation, which is the major reversible OPTM involved in redox signaling. (4) We did not investigate the role of SirT1 oxidation in apoptosis, senescence, inflammation, or other known molecular processes associated with AA. Nonetheless, our study strongly suggests that prevention of reversible oxidation of SirT1 could be a novel therapeutic strategy to preserve SirT1 activity in the vasculature to prevent MMP activation and ameliorate TAA in MFS. Further research on the role of

rOPTM of proteins in AA is necessary and may be critical to prevention of deaths from AA dissections and ruptures, for which there is currently no cure.

Supplementary Material

Refer to Web version on PubMed Central for supplementary material.

ACKNOWLEDGEMENTS

We would like to thank the Boston University Medical Campus Analytical Instrumentation (Drs. Lynn Deng and Matthew Au) and Cellular Imaging Cores (Dr. Michael Kirber), Drs. Vladimir Mastuyugin and Syed Husain Mustafa Rizvi for their expert technical support and suggestions. We thank Mr. Ryan Liu and Ms. Hannah Guo for their assistance with aortic immunostainings and aortic diameter measurements. We would also like to thank the Aortic Valve Operative Outcomes in Marfan Patients study (Principal Investigator Dr. Joseph S. Coselli, Director of the Genetic Repository Dr. Diana M. Milewicz), sponsored by the Marfan Foundation, Baylor College of Medicine, and Stanford University, for providing aortic samples used in this study. The Marfan Foundation received support from Vascutek, Ltd., St. Jude Medical, Inc., the Macquet Cardiovascular/Getinge Group, and Broccoli Center for Aortic Disease, John Hopkins Medicine. The figure for the graphical abstract was created with BioRender.com.

FUNDING SOURCES

This work was supported by NIH R01 grants HL136311 to FS, HL137771 to JH; R21 grants AA026922 and AG058983 to JH; NIH T32 training grant HL007224 to JBG; a Marfan Foundation Early-Stage Investigator grant to FS, and a BU CTSI Integrated Pilot grant 1UL1TR001430 to FS and JH.

Non-standard Abbreviations and Acronyms

AA	Aortic aneurysm
AAV	Adeno-associated virus
DHE	Dihydroethidium
rOPTM	Reversible oxidative post-translational modifications
Fbn1^{mgR/mgR}	Fibrillin-1 mutant mice (hypomorphic Fbn1 ^{mgR/mgR} mice)
Glrx	Glutaredoxin-1
MFS	Marfan syndrome
MMP	Matrix metalloproteinase
Pr-SSG	<i>S</i> -glutathionylated proteins
ROS	Reactive oxygen species
ReOx SirT1	Reversibly oxidized SirT1
SirT1	Sirtuin-1
VSMCs	Vascular smooth muscle cells
TGFβ1	Transforming growth factor beta 1
TAA	Thoracic aortic aneurysm

VSM

Vascular smooth muscle

REFERENCES

1. Virani SS, Alonso A, Aparicio HJ, et al. American Heart Association Council on Epidemiology and Prevention Statistics Committee and Stroke Statistics Subcommittee. Heart Disease and Stroke Statistics-2021 Update: A Report From the American Heart Association. *Circulation*. 2021;143:e254–e743. [PubMed: 33501848]
2. Zúñiga-Muñoz AM, Pérez-Torres I, Guarner-Lans V, Núñez-Garrido E, Velázquez Espejel R, Huesca-Gómez C, Gamboa-Ávila R, Soto ME. Glutathione system participation in thoracic aneurysms from patients with Marfan syndrome. *Vasa*. 2017;46:177–186. [PubMed: 28173744]
3. You W, Hong Y, He H, Huang X, Tao W, Liang X, Zhang Y, Li X. TGF- β mediates aortic smooth muscle cell senescence in Marfan syndrome. *Aging*. 2019;11:3574–3584. [PubMed: 31147528]
4. Jiménez-Altayó F, Meirelles T, Crosas-Molist E, et al. Redox stress in Marfan syndrome: Dissecting the role of the NADPH oxidase NOX4 in aortic aneurysm. *Free Radic Biol Med*. 2018;118:44–58. [PubMed: 29471108]
5. Pizzino G, Irrera N, Cucinotta M, Pallio G, Mannino F, Arcoraci V, Squadrito F, Altavilla D, Bitto A. Oxidative Stress: Harms and Benefits for Human Health. *Oxid Med Cell Longev*. 2017;2017:8416763. [PubMed: 28819546]
6. Burgoyne JR, Mongue-Din H, Eaton P, Shah AM. Redox signaling in cardiac physiology and pathology. *Circ Res*. 2012;111:1091–106. [PubMed: 23023511]
7. Rashdan NA, Shrestha B, Pattillo CB. S-glutathionylation, friend or foe in cardiovascular health and disease. *Redox Biol*. 2020;37:101693. [PubMed: 32912836]
8. Haigis MC, Sinclair DA. Mammalian sirtuins: biological insights and disease relevance. *Annu Rev Pathol*. 2010;5:253–295. [PubMed: 20078221]
9. Gorenne I, Kumar S, Gray K, Figg N, Yu H, Mercer J, Bennett M. Vascular smooth muscle cell sirtuin 1 protects against DNA damage and inhibits atherosclerosis. *Circulation*. 2013;127:386–396. [PubMed: 23224247]
10. Li L, Zhang HN, Chen HZ, et al. SIRT1 acts as a modulator of neointima formation following vascular injury in mice. *Circ Res*. 2011;108:1180–1189. [PubMed: 21474819]
11. Gao P, Xu TT, Lu J, Li L, Xu J, Hao DL, Chen HZ, Liu DP. Overexpression of SIRT1 in vascular smooth muscle cells attenuates angiotensin II-induced vascular remodeling and hypertension in mice. *J Mol Med (Berl)*. 2014;92:347–357. [PubMed: 24352856]
12. Chen H-Z, Wang F, Gao P, et al. Age-Associated Sirtuin 1 Reduction in Vascular Smooth Muscle Links Vascular Senescence and Inflammation to Abdominal Aortic Aneurysm. *Circ Res*. 2016;119:1076–1088. [PubMed: 27650558]
13. Fry JL, Shiraishi Y, Turcotte R, et al. Vascular Smooth Muscle Sirtuin-1 Protects Against Aortic Dissection During Angiotensin II-Induced Hypertension. *J Am Heart Assoc*. 2015;4:e002384. [PubMed: 26376991]
14. Pereira L, Lee SY, Gayraud B, Andrikopoulos K, Shapiro SD, Bunton T, Biery NJ, Dietz HC, Sakai LY, Ramirez F. Pathogenetic sequence for aneurysm revealed in mice underexpressing fibrillin-1. *Proc Natl Acad Sci U S A*. 1999;96:3819–3823. [PubMed: 10097121]
15. Xiong W, Meisinger T, Knispel R, Worth JM, Baxter BT. MMP-2 regulates Erk1/2 phosphorylation and aortic dilatation in Marfan syndrome. *Circ Res*. 2012;110:e92–e101. [PubMed: 22550139]
16. Cook JR, Clayton NP, Carta L, Galatioto J, Chiu E, Smaldone S, Nelson CA, Cheng SH, Wentworth BM, Ramirez F. Dimorphic Effects of Transforming Growth Factor- β Signaling During Aortic Aneurysm Progression in Mice Suggest a Combinatorial Therapy for Marfan Syndrome Significance. *Arterioscler Thromb Vasc Biol*. 2015;35:911–917. [PubMed: 25614286]
17. Pedroza AJ, Tashima Y, Shad R, et al. Single-Cell Transcriptomic Profiling of Vascular Smooth Muscle Cell Phenotype Modulation in Marfan Syndrome Aortic Aneurysm. *Arterioscler Thromb Vasc Biol*. 2020;40:2195–2211. [PubMed: 32698686]
18. Walter W, Sánchez-Cabo F, Ricote M. GOplot: an R package for visually combining expression data with functional analysis. *Bioinformatics*. 2015;31:2912–4. [PubMed: 25964631]

19. Shao D, Han J, Hou X, et al. Glutaredoxin-1 Deficiency Causes Fatty Liver and Dyslipidemia by Inhibiting Sirtuin-1. *Antioxid Redox Signal*. 2017;27:313–327. [PubMed: 27958883]
20. Han J, Weisbrod RM, Shao D, et al. The redox mechanism for vascular barrier dysfunction associated with metabolic disorders: Glutathionylation of Rac1 in endothelial cells. *Redox Biol*. 2016;9:306–319. [PubMed: 27693992]
21. Kimura T, Ferran B, Tsukahara Y, et al. Production of adeno-associated virus vectors for in vitro and in vivo applications. *Sci Rep*. 2019;9:13601. [PubMed: 31537820]
22. Seidel K, Wan X, Zhang M, Zhou Y, Zang M, Han J. Alcohol Binge Drinking Selectively Stimulates Protein S-Glutathionylation in Aorta and Liver of ApoE $-/-$ Mice. *Front Cardiovasc Med*. 2021;8:649813. [PubMed: 33796575]
23. Lee M-J, Pickering RT, Shibad V, Wu Y, Karastergiou K, Jager M, Layne MD, Fried SK. Impaired Glucocorticoid Suppression of TGF β Signaling in Human Omental Adipose Tissues Limits Adipogenesis and May Promote Fibrosis. *Diabetes*. 2019;68:587–597. [PubMed: 30530781]
24. Zhou Y, Wan X, Seidel K, Zhang M, Goodman JB, Seta F, Hamburg N, Han J. Aging and Hypercholesterolemia Differentially Affect the Unfolded Protein Response in the Vasculature of ApoE $-/-$ Mice. *J Am Heart Assoc*. 2021;10:e020441. [PubMed: 34533042]
25. Clempus RE, Griendling KK. Reactive oxygen species signaling in vascular smooth muscle cells. *Cardiovasc Res*. 2006;71:216–25. [PubMed: 16616906]
26. D'Autréaux B, Toledano MB. ROS as signalling molecules: mechanisms that generate specificity in ROS homeostasis. *Nat Rev Mol Cell Biol*. 2007;8:813–24. [PubMed: 17848967]
27. Xiong Y, Uys JD, Tew KD, Townsend DM. S-glutathionylation: from molecular mechanisms to health outcomes. *Antioxid Redox Signal*. 2011;15:233–70. [PubMed: 21235352]
28. Cheng HL, Mostoslavsky R, Saito S, Manis JP, Gu Y, Patel P, Bronson R, Appella E, Alt FW, Chua KF. Developmental defects and p53 hyperacetylation in Sir2 homolog (SIRT1)-deficient mice. *Proc Natl Acad Sci U S A*. 2003;100:10794–10799. [PubMed: 12960381]
29. Borra MT, Smith BC, Denu JM. Mechanism of Human SIRT1 Activation by Resveratrol. *Journal of Biological Chemistry*. 2005;280:17187–17195. [PubMed: 15749705]
30. Rabkin SW. The Role Matrix Metalloproteinases in the Production of Aortic Aneurysm. *Prog Mol Biol Transl Sci*. 2017;147:239–265. [PubMed: 28413030]
31. Liao M, Liu Z, Bao J, et al. A proteomic study of the aortic media in human thoracic aortic dissection: implication for oxidative stress. *J Thorac Cardiovasc Surg*. 2008;136:65–72, 72.e1–3. [PubMed: 18603055]
32. Miller FJ, Sharp WJ, Fang X, Oberley LW, Oberley TD, Weintraub NL. Oxidative stress in human abdominal aortic aneurysms: a potential mediator of aneurysmal remodeling. *Arterioscler Thromb Vasc Biol*. 2002;22:560–5. [PubMed: 11950691]
33. Pincemail J, Defraigne JO, Cheramy-Bien JP, Dardenne N, Donneau AF, Albert A, Labropoulos N, Sakalihasan N. On the potential increase of the oxidative stress status in patients with abdominal aortic aneurysm. *Redox Rep*. 2012;17:139–44. [PubMed: 22732574]
34. van der Pluijm I, Burger J, van Heijningen PM, et al. Decreased mitochondrial respiration in aneurysmal aortas of Fibulin-4 mutant mice is linked to PGC1A regulation. *Cardiovasc Res*. 2018;114:1776–1793. [PubMed: 29931197]
35. Siu KL, Li Q, Zhang Y, Guo J, Youn JY, Du J, Cai H. NOX isoforms in the development of abdominal aortic aneurysm. *Redox Biol*. 2017;11:118–125. [PubMed: 27912196]
36. Shelton MD, Chock PB, Mieryl JJ. Glutaredoxin: role in reversible protein s-glutathionylation and regulation of redox signal transduction and protein translocation. *Antioxid Redox Signal*. 2005;7:348–66. [PubMed: 15706083]
37. Matsui R, Ferran B, Oh A, Croteau D, Shao D, Han J, Pimentel DR, Bachschmid MM. Redox Regulation via Glutaredoxin-1 and Protein S-Glutathionylation. *Antioxid Redox Signal*. 2020;32:677–700. [PubMed: 31813265]
38. Neptune ER, Frischmeyer PA, Arking DE, Myers L, Bunton TE, Gayraud B, Ramirez F, Sakai LY, Dietz HC. Dysregulation of TGF-beta activation contributes to pathogenesis in Marfan syndrome. *Nat Genet*. 2003;33:407–411. [PubMed: 12598898]
39. Ford CM, Li S, Pickering JG. Angiotensin II stimulates collagen synthesis in human vascular smooth muscle cells. Involvement of the AT(1) receptor, transforming growth factor-beta,

- and tyrosine phosphorylation. *Arterioscler Thromb Vasc Biol.* 1999;19:1843–1851. [PubMed: 10446062]
40. Sturrock A, Cahill B, Norman K, et al. Transforming growth factor-beta1 induces Nox4 NAD(P)H oxidase and reactive oxygen species-dependent proliferation in human pulmonary artery smooth muscle cells. *Am J Physiol Lung Cell Mol Physiol.* 2006;290:L661–L673. [PubMed: 16227320]
41. Chen X, Lu H, Rateri DL, Cassis LA, Daugherty A. Conundrum of angiotensin II and TGF-beta interactions in aortic aneurysms. *Curr Opin Pharmacol.* 2013;13:180–185. [PubMed: 23395156]
42. Chen X, Rateri DL, Howatt DA, Balakrishnan A, Moorlegghen JJ, Cassis LA, Daugherty A. TGF- β neutralization enhances angii-induced aortic rupture and aneurysm in both thoracic and abdominal regions. *PLoS One.* 2016. doi:10.1371/journal.pone.0153811.
43. Wang Y, Ait-Oufella H, Herbin O, et al. TGF-beta activity protects against inflammatory aortic aneurysm progression and complications in angiotensin II-infused mice. *J Clin Invest.* 2010;120:422–432. [PubMed: 20101093]
44. Habashi JP, Judge DP, Holm TM, et al. Losartan, an AT1 antagonist, prevents aortic aneurysm in a mouse model of Marfan syndrome. *Science (1979).* 2006;312:117–121.
45. Franken R, den Hartog AW, Radonic T, et al. Beneficial Outcome of Losartan Therapy Depends on Type of FBN1 Mutation in Marfan Syndrome CLINICAL PERSPECTIVE. *Circ Cardiovasc Genet.* 2015;8:383–388. [PubMed: 25613431]
46. Brooke BS, Habashi JP, Judge DP, Patel N, Loeys B, Dietz HC. Angiotensin II blockade and aortic-root dilation in Marfan's syndrome. *N Engl J Med.* 2008;358:2787–2795. [PubMed: 18579813]
47. Marchioli R, Schweiger C, Levantesi G, Tavazzi L, Valagussa F. Antioxidant vitamins and prevention of cardiovascular disease: epidemiological and clinical trial data. *Lipids.* 2001;36 Suppl:S53–63. [PubMed: 11837994]
48. Fry JL, al Sayah L, Weisbrod RM, van Roy I, Weng X, Cohen RA, Bachschmid MM, Seta F. Vascular Smooth Muscle Sirtuin-1 Protects Against Diet-Induced Aortic Stiffness. *Hypertension.* 2016;68:775–784. [PubMed: 27432859]
49. Guarente L. Calorie restriction and SIR2 genes--towards a mechanism. *Mech Ageing Dev.* 2005;126:923–928. [PubMed: 15941577]
50. Liu Y, Wang T-T, Zhang R, et al. Calorie restriction protects against experimental abdominal aortic aneurysms in mice. *J Exp Med.* 2016;213:2473–2488. [PubMed: 27670594]
51. Hibender S, Franken R, van Roomen C, et al. Resveratrol Inhibits Aortic Root Dilatation in the Fbn1C1039G/+ Marfan Mouse Model. *Arterioscler Thromb Vasc Biol.* 2016;36:1618–26. [PubMed: 27283746]
52. Zee RS, Yoo CB, Pimentel DR, Perlman DH, Burgoyne JR, Hou X, McComb ME, Costello CE, Cohen RA, Bachschmid MM. Redox regulation of sirtuin-1 by S-glutathiolation. *Antioxid Redox Signal.* 2010;13:1023–1032. [PubMed: 20392170]
53. Shao D, Yao C, Kim MH, Fry J, Cohen RA, Costello CE, Matsui R, Seta F, McComb ME, Bachschmid MM. Improved mass spectrometry-based activity assay reveals oxidative and metabolic stress as sirtuin-1 regulators. *Redox Biol.* 2019;22:101150. [PubMed: 30877853]
54. Shao D, Fry JL, Han J, Hou X, Pimentel DR, Matsui R, Cohen RA, Bachschmid MM. A redox-resistant sirtuin-1 mutant protects against hepatic metabolic and oxidant stress. *J Biol Chem.* 2014;289:7293–306. [PubMed: 24451382]

HIGHLIGHTS

- Reversible oxidative post-translational modifications (rOPTM) of proteins, mainly *S*-glutathionylation, were significantly increased in aortas and VSM cells of *fibrillin-1* mutant mice ($Fbn1^{mgR/mgR}$), a model of Marfan syndrome (MFS) prone to thoracic aortic aneurysms and ruptures, which closely mimics the human aneurysmal pathology.
- Reversible OPTM of sirtuin-1 (SirT1), a lysine deacetylase essential for aortic wall structural integrity, were significantly increased in $Fbn1^{mgR/mgR}$ VSMCs or after treatment with TGF β 1, a cytokine associated with MFS, and in VSMCs with deletion of glutaredoxin-1 (Glrx), the thiol transferase that specifically removes GSH adducts from protein cysteines.
- Reversible SirT1 OPTM and downstream activation of matrix metalloproteinases, mainly MMP2 and MMP9, in $Fbn1^{mgR/mgR}$ VSMCs were decreased by overexpression of Glrx or a redox-resistant SirT1.

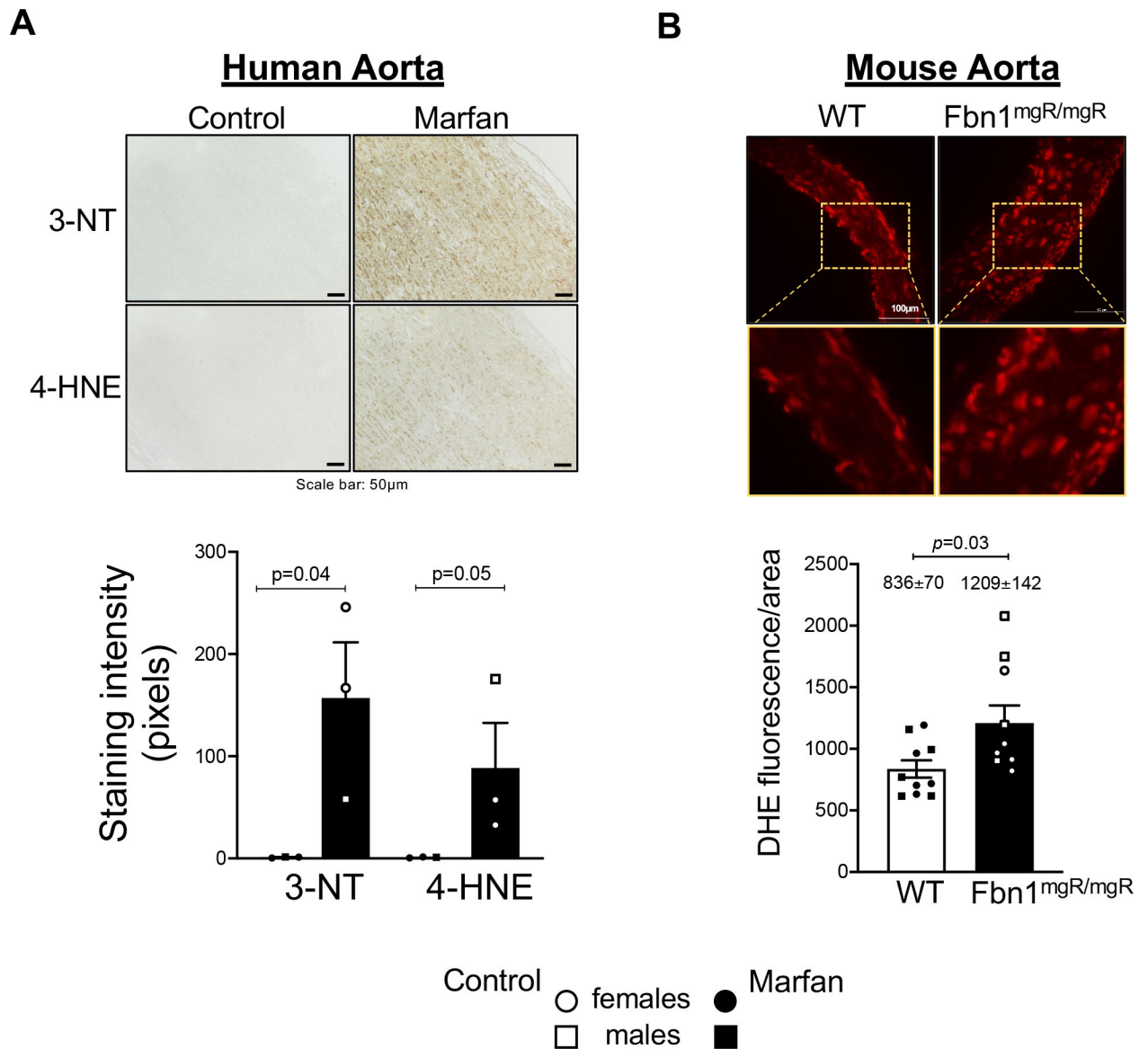
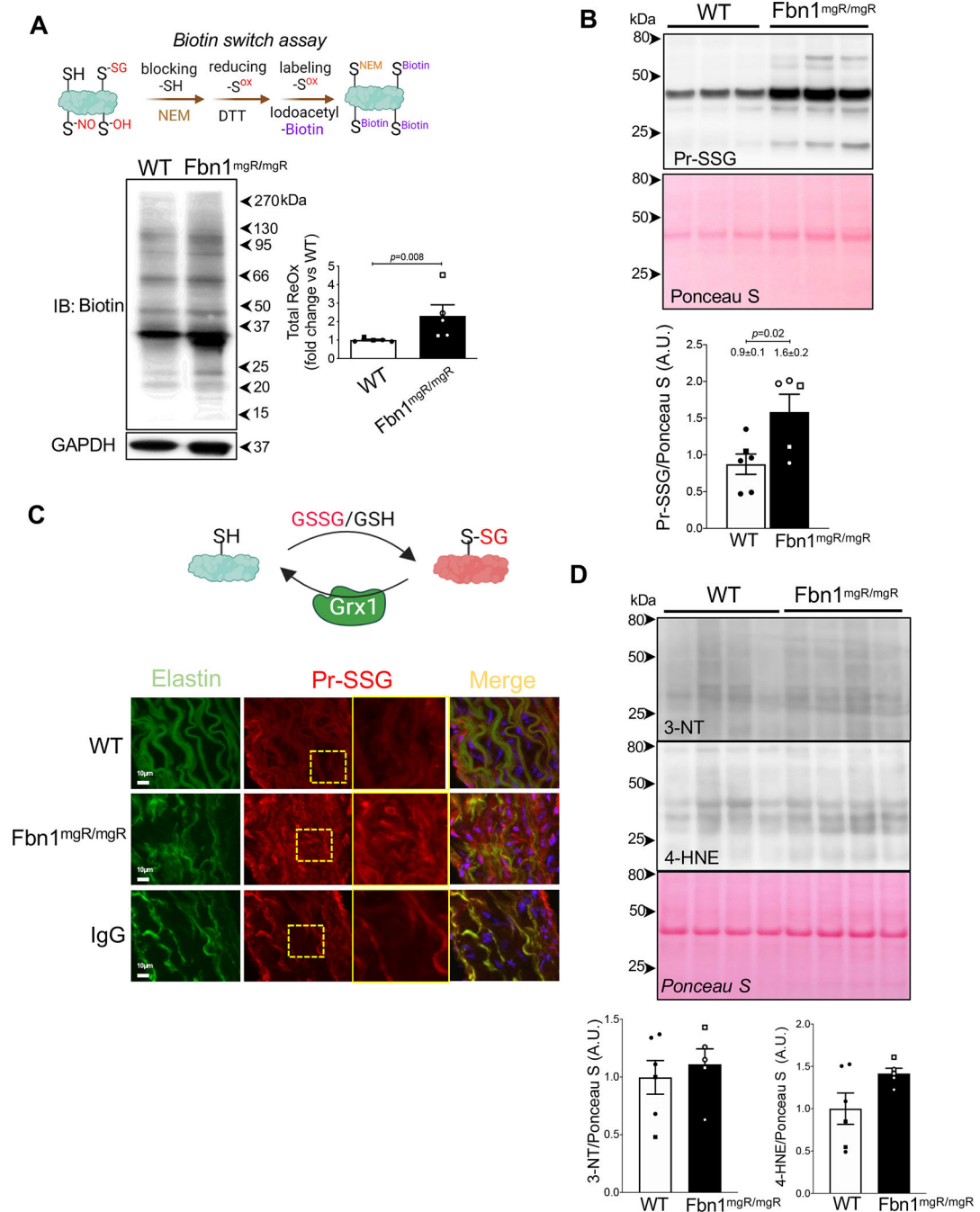


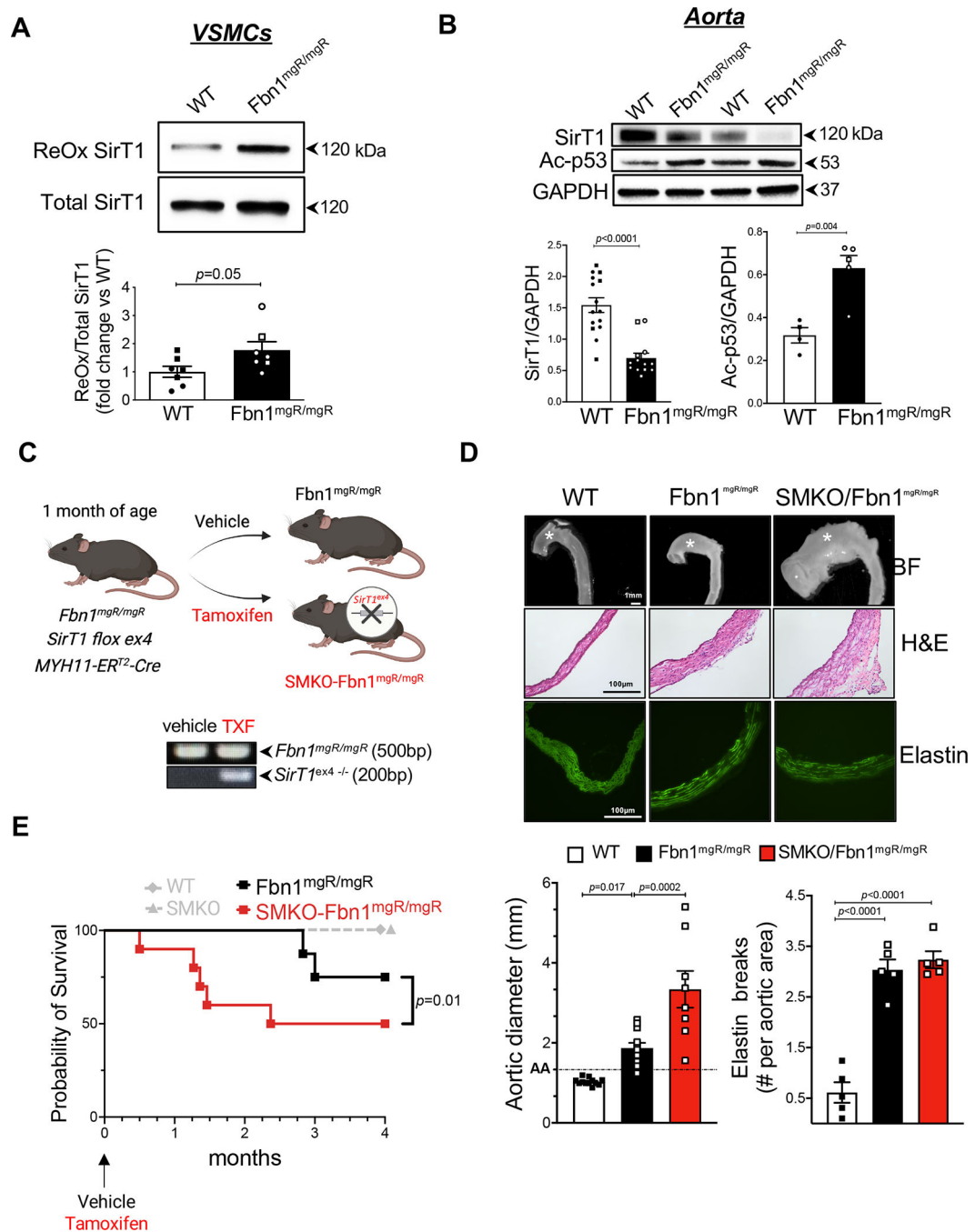
Figure 1.

(A) Representative images of human aortic sections, from healthy (n=3) and Marfan (n=3) donors (*circles*, females; *squares*, males), stained for 3-nitrotyrosine (3-NT) and 4-hydroxynonenal (4-HNE), two indices of reactive oxygen species (ROS)-mediated oxidation of proteins and lipids, respectively. Quantitation of immunostaining signal in graph. Data expressed as fold change vs controls; $p=0.04$ for 3-NT, $p=0.05$ for 4-HNE, nested unpaired t-test. Scale bar = 50 μ m. (B) ROS, mainly superoxide anion, assessed using DHE staining in aortic sections from WT (n=10) and Fbn1^{mgR/mgR} (n=10) mice (*circles*, females; *squares*, males); $p=0.03$, unpaired Student's t-test. Scale bar = 100 μ m. Representative regions with intense DHE signal are magnified in the yellow box.

**Figure 2.**

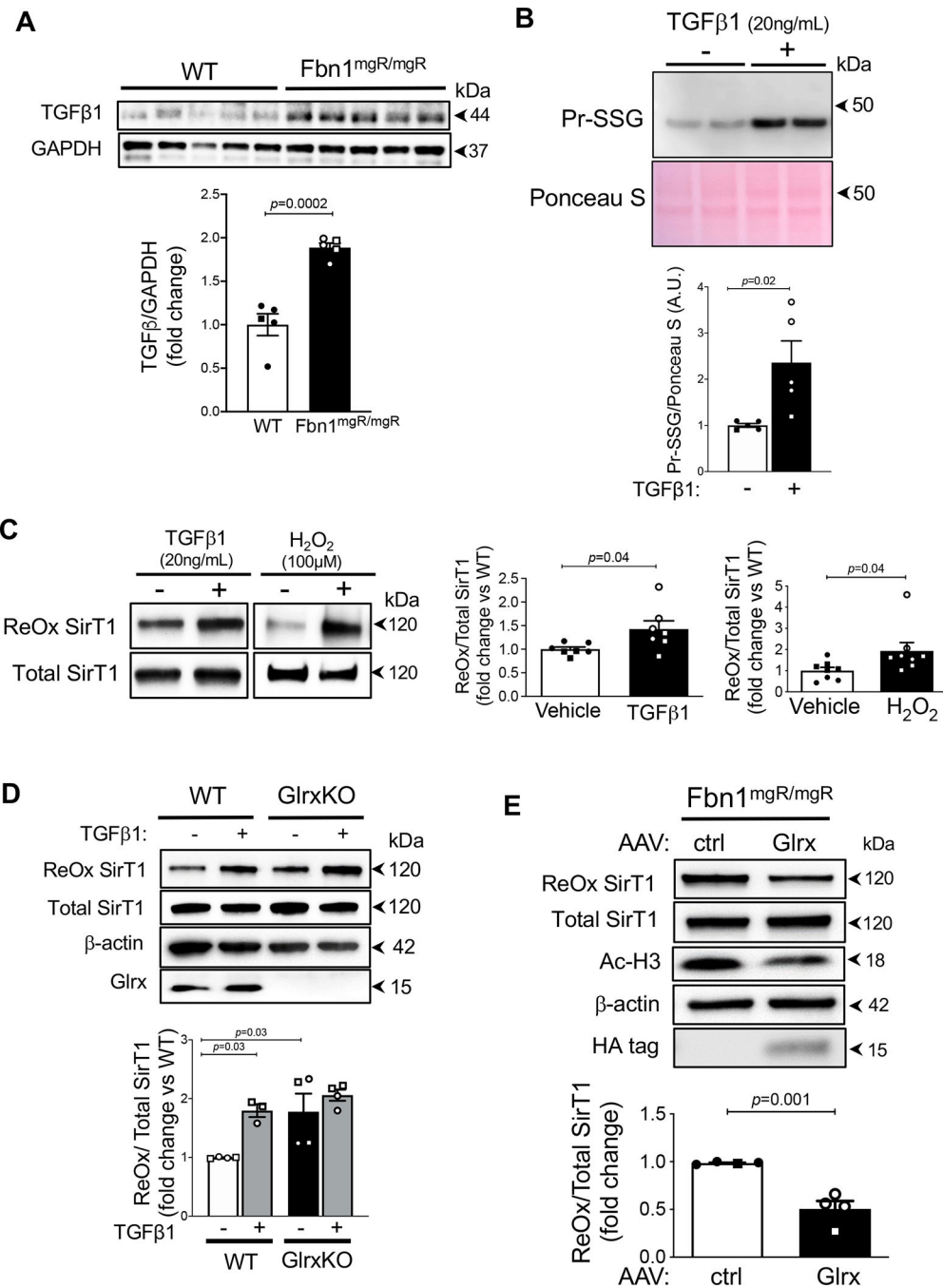
(A) Representative Western blot of total reversible oxidation of proteins (total ReOx) in aortas of WT (n=5) and Fbn1^{mgR/mgR} (n=5) mice (*circles*, females; *squares*, males), measured using a biotin switch assay, as described in Materials & Methods. β -actin was used as loading control. The graph shows band intensity quantitation, and data are expressed as fold change versus WT; $p=0.008$, Mann-Whitney non-parametric test. (B) Representative Western blot of total protein glutathionylation (Pr-SSG), a form of reversible oxidation, in aortas of WT (n=6) and Fbn1^{mgR/mgR} (n=5) mice (*circles*, females; *squares*, males).

The graph shows quantitative results of Pr-SSG band intensities expressed as the ratio of corresponding Ponceau S membrane staining. Each lane represents one mouse; $p=0.02$, unpaired Student's t-test. **(C)** Representative images, acquired at 40× magnification, of aortic sections from WT (n=3) and Fbn1^{mgR/mgR} (n=3) mice after immunostaining with an anti-Pr-SSG antibody (scale bar: 10 μm). Elastin autofluorescence (*in green*) is shown to delineate the aortic wall. Representative regions with intense Pr-SSG signal are magnified in the yellow box. IgG indicates mouse IgG used as negative control for antibody specificity. **(D)** Representative Western blot of 3-nitrotyrosine (3-NT) and 4-hydroxynonenal (4-HNE), two indices of ROS-mediated irreversible oxidation of protein residues, in aortas of WT (n=6) and Fbn1^{mgR/mgR} (n=5) mice (*circles*, females; *squares*, males). Each lane represents one mouse. Quantitation in graphs indicates 3-NT and 4-HNE band intensities expressed as ratio of corresponding Ponceau S membrane staining ($p=0.58$ and $p=0.08$, respectively, by unpaired Student's t-test).

**Figure 3.**

(A) Biotin switch assay to detect reversibly oxidized SirT1 (ReOx SirT1) in WT and Fbn1^{mgR/mgR} VSMCs; $n=7$ replicate experiments. *Circles* and *squares* indicate VSMCs isolated from females and males mice, respectively. Band intensity quantitation, summarized in the graph, were calculated as the ratio of total SirT1 and expressed as fold change versus WT, for each experiment; $p=0.05$, unpaired Student's t-test. (B) Representative Western blots for SirT1 and acetylated p53 at lysine 379 (Ac-p53), an index of SirT1 activity, in aortas of WT ($n=4-15$) and Fbn1^{mgR/mgR} ($n=5-13$) mice (*circles*, females; *squares*,

males); $p < 0.0001$ and $p = 0.004$, respectively, by unpaired Student's t-test. **(C)** Graphic representation of Fbn1^{mgR/mgR} mice with tamoxifen-inducible VSM-specific SirT1 deletion (SMKO-Fbn1^{mgR/mgR}) and littermates (vehicle-treated) Fbn1^{mgR/mgR} mice. Genotype PCR on biopsied tail DNA confirmed the presence of the Fbn1^{mgR/mgR} allele (500bp band) in both vehicle- and tamoxifen-treated Fbn1^{mgR/mgR} mice and the SirT1^{ex4} deletion (200bp band) after tamoxifen in SMKO-Fbn1^{mgR/mgR} mice. **(D) Top:** Representative images of aortas, taken in bright field (BF), from WT, Fbn1^{mgR/mgR} and SMKO-Fbn1^{mgR/mgR} mice (all males) showing severe TAA in SMKO-Fbn1^{mgR/mgR}. Asterisk indicates TAA. Scale bar = 1mm. **Bottom:** Representative images, taken at 20× magnification, of H&E-stained aortic sections and elastin laminae, captured as autofluorescence at 488nm, in WT, Fbn1^{mgR/mgR} and SMKO-Fbn1^{mgR/mgR} mice. Scale bar = 100 μm. Graphs indicate aortic diameter and elastin fragmentation in WT (n=12), Fbn1^{mgR/mgR} (n=12) and SMKO-Fbn1^{mgR/mgR} (n=8) mice, measured at necropsy; $p = 0.017$, WT vs Fbn1^{mgR/mgR}; $p = 0.0002$ Fbn1^{mgR/mgR} vs SMKO/Fbn1^{mgR/mgR}; $p < 0.0001$ Fbn1^{mgR/mgR} or SMKO/Fbn1^{mgR/mgR} vs WT; one-way ANOVA with Tukey's multiple comparisons test. Horizontal line in graph indicates the threshold for AA, defined as an increase in aortic diameter >150% of WT diameter. **(E)** Survival curve of WT (n=8), SMKO (n=8), Fbn1^{mgR/mgR} (n=8) and SMKO-Fbn1^{mgR/mgR} (n=10) mice after vehicle or tamoxifen administration, respectively; $p = 0.01$; Log-rank (Mantel-Cox) test.

**Figure 4.**

(A) Western blot of aortas from WT (n=5) and Fbn1^{mgR/mgR} (n=5) mice (*circles*, females; *squares*, males) indicating increased levels of TGFβ in Fbn1^{mgR/mgR} aortas. GAPDH was used as the loading control. Each lane represents one mouse. Quantitation of band intensities shown in graph; $p=0.0002$, unpaired Student's t-test. (B) Representative Western blot of total protein glutathionylation (Pr-SSG) in VSMCs from WT mice treated with vehicle or TGFβ1 (20 ng/mL). *Circles* and *squares* indicate VSMCs isolated from females and males mice, respectively. n=5 replicate experiments; $p=0.02$, unpaired Student's t-test. (C)

Representative Western blots of reversibly oxidized SirT1 (ReOx SirT1) in VSMCs after overnight treatment with 20 ng/mL TGF β 1; n=7 replicate experiments; $p=0.04$, unpaired Student's t-test; or 15 min treatment with 100 μ M H₂O₂; n=8 replicate experiments; $p=0.04$, unpaired Student's t-test. Samples were subjected to a biotin switch assay, as described in Materials & Methods. *Circles* and *squares* indicate VSMCs isolated from females and males mice, respectively. **(D)** Biotin switch assay for ReOx SirT1 in VSMCs from WT and Glx-null mice (GlxKO), treated overnight with vehicle or TGF β 1 (20 ng/mL); n=4 replicate experiments with VSMCs isolated from 4 female (*circles*) and 4 male (*squares*) WT or GlxKO mice; $p=0.03$ WT/vehicle vs WT/TGF β 1 and $p=0.03$ WT/vehicle vs GlxKO/vehicle, two-way ANOVA with Tukey's multiple comparisons post hoc test. **(E)** Overexpression of Glrx using an AAV (8.2×10^7 vg/ μ L) in Fbn1^{mgR/mgR} VSMCs decreased SirT1 reversible oxidation, as measured using a biotin switch assay, and decreased histone 3 (H3) acetylated at lysine 9 (Ac-H3^{lys9}), an index of SirT1 activity, compared to a control AAV. β -actin used as loading control. HA tag confirms overexpressed Glrx. n=4 replicate experiments with VSMCs isolated from 4 female (*circles*) or male (*squares*) Fbn1^{mgR/mgR} mice; $p=0.001$, unpaired Student's t-test.

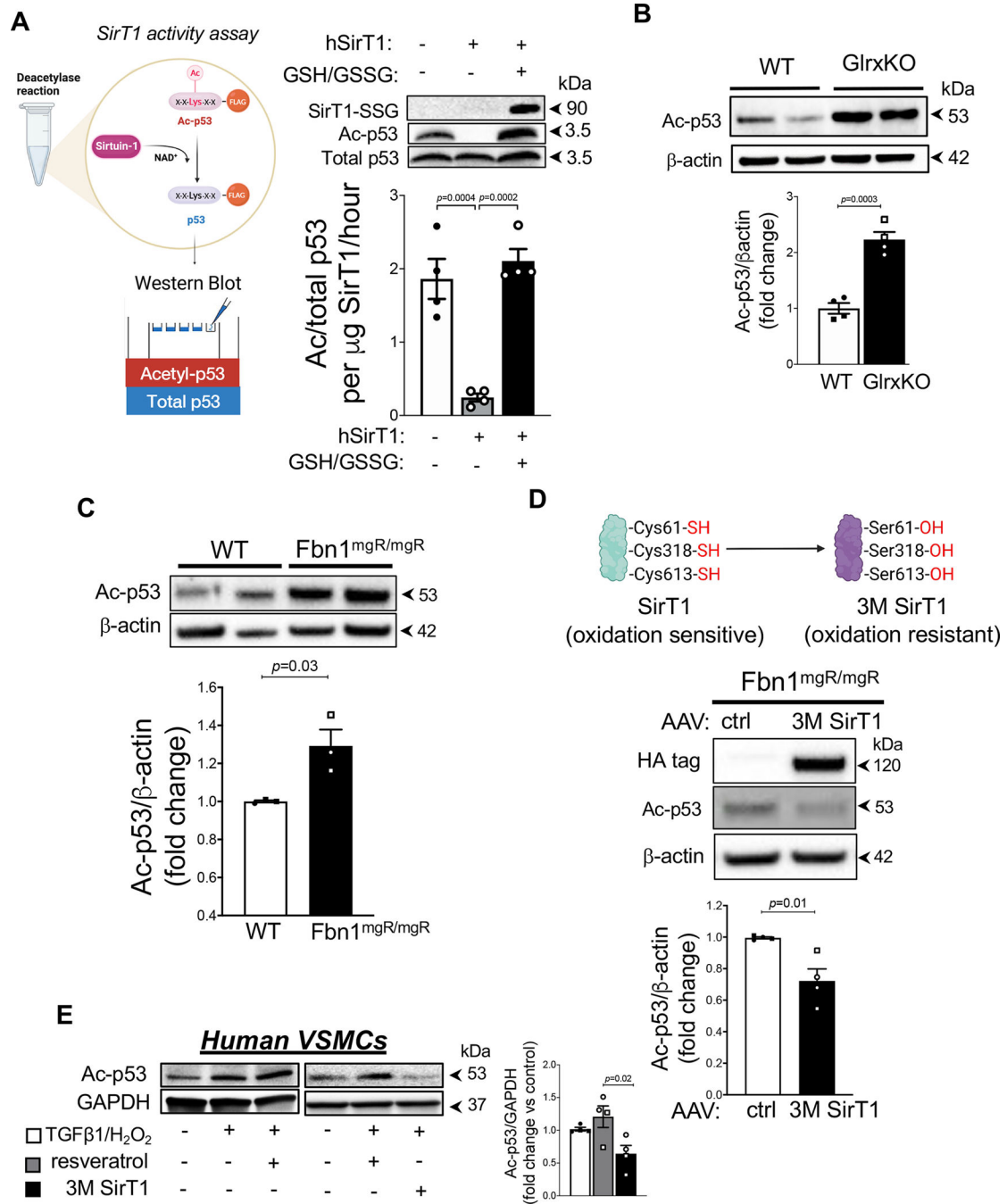
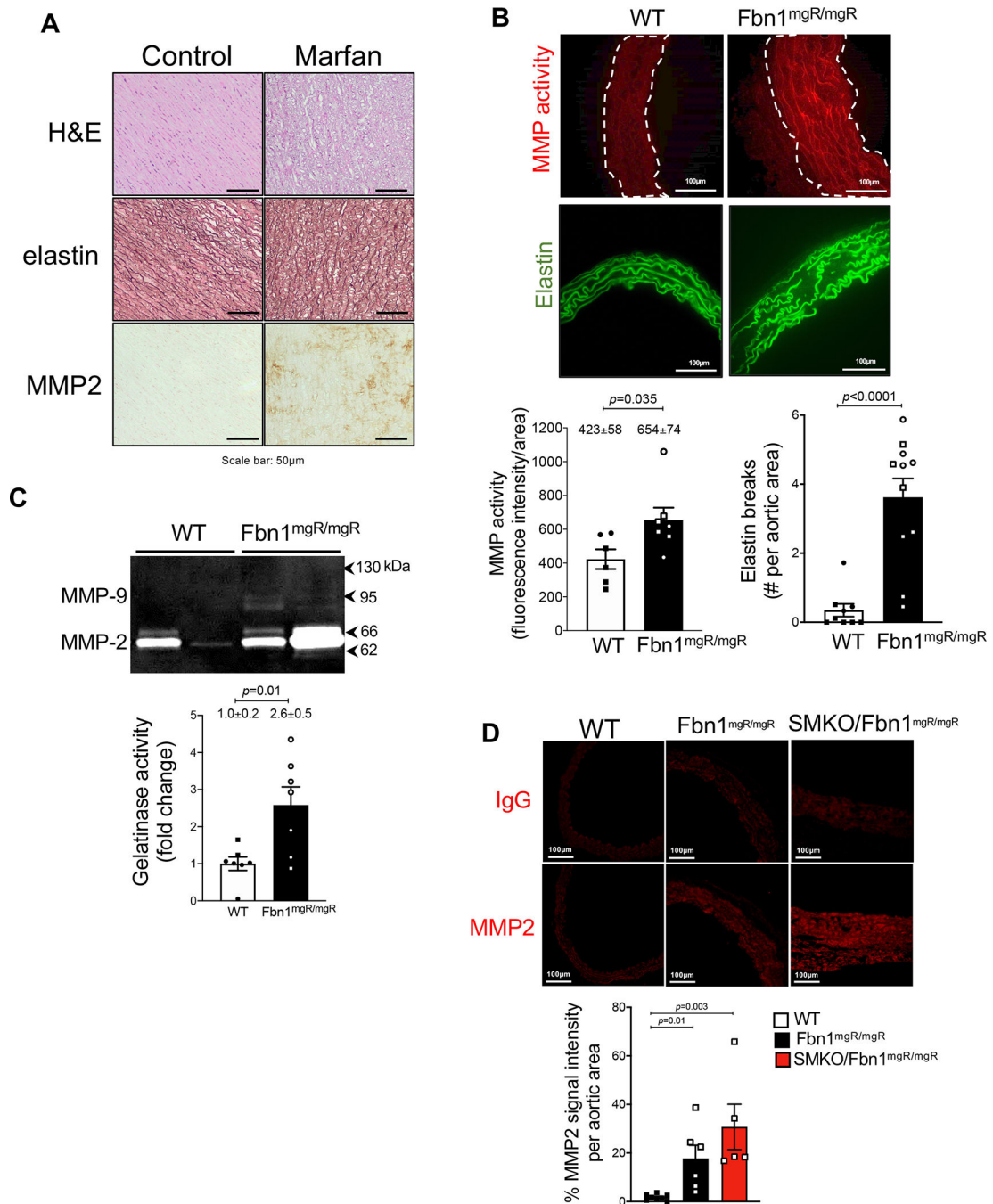


Figure 5.

(A) Treatment of human recombinant SirT1 (750ng) with GSH/GSSG (20 mM/5 mM) inhibited SirT1 activity. Anti-FLAG antibody was used to detect total p53 and an anti-GSH antibody was used to detect glutathionylated recombinant SirT1 (SirT1-SSG). Data were calculated as ratio of band intensities for acetylated and total p53, which was used as an indicator of SirT1 deacetylase activity and expressed per μ g SirT1 per hour. n=4 replicate experiments; $p=0.0004$ control vs SirT1; $p=0.0002$ SirT1 vs SirT1/GSSG, one-way ANOVA with Tukey's multiple comparisons post hoc test. (B) Representative Western blot for

acetylated p53 (Ac-p53), an index of SirT1 activity, in WT and GlrxKO VSMCs. β -actin used as loading control. Quantification of band intensities is shown in the graph; n=4 replicate experiments with VSMCs isolated from 4 female (*circles*) and 4 male (*squares*) WT or GlrxKO mice; $p=0.0003$, unpaired Student's t-test. **(C)** Representative Western blot for SirT1 and acetylated p53 (Ac-p53) in WT and Fbn1^{mgR/mgR} VSMCs. β -actin used as loading control. Quantification of band intensities is shown in the graph; n=3 replicate experiments with VSMCs isolated from 3 WT and 3 Fbn1^{mgR/mgR} mice (*circles*, females; *squares*, males); $p=0.03$, unpaired Student's t-test. **(D)** Representative Western blot for SirT1 and acetylated p53 in Fbn1^{mgR/mgR} VSMCs treated with a control or 3M SirT1 AAV. Quantitation of band intensities is shown in the graph; n=4 replicate experiments with VSMCs isolated from 4 female (*circles*) and 4 male (*squares*) Fbn1^{mgR/mgR} mice; $p=0.01$, unpaired Student's t-test. **(E)** Representative Western blot for SirT1 and acetylated p53 (Ac-p53) in human VSMCs treated with TGF β 1 (20 ng/mL, overnight) and H₂O₂ (100 μ M, 15 min), with or without the SirT1 activator resveratrol (10 μ M, 2 hrs), 3M SirT1 AAV (1.3 \times 10¹⁰ vg) or left untreated (control). GAPDH used as loading control. n=4 replicate experiments with VSMCs from 4 female (*circles*) or male (*squares*) donors; $p=0.02$, one-way ANOVA with Tukey's multiple comparison test.

**Figure 6.**

(A) Representative images of aortic sections from healthy donors (n=3) or individuals with Marfan syndrome (n=3), stained with H&E, elastin stain and MMP2, as described in Materials & Methods. Scale bar = 50 μ m. (B) Representative images of MMP activity on aortic sections from WT (n=6) and Fbn1^{mgR/mgR} (n=7) mice. The immunofluorescent red signal is indicative of MMP activity measured *in situ* with a specific MMP substrate, which fluoresces upon specific cleavage by active MMPs. Signal intensity was quantified using ImageJ and normalized to the aortic area for each mouse, as shown in the graph; $p=0.03$,

unpaired Student's t-test. Green signal indicates elastin autofluorescence at 488 nm in aortic cryosections, acquired at 40× magnification, in WT (n=9) and Fbn1^{mgR/mgR} (n=11) aortas. Elastin fragmentation was quantified manually as described in Materials & Methods. Scale bar = 100 μm; $p < 0.0001$, unpaired Student's t-test. *Circles* and *squares* indicate female and male mice, respectively. **(C)** Representative images of in-gel zymography of culture medium from WT and Fbn1^{mgR/mgR} VSMCs; data are expressed as fold change of pg gelatinase activity per μg protein. n=7 replicate experiments with VSMCs isolated from 7 WT and 7 Fbn1^{mgR/mgR} mice (*circles*, females; *squares*, males); $p = 0.01$, unpaired Student's t-test. **(D)** Representative images of MMP2 immunostaining on aortic sections from WT (n=8), Fbn1^{mgR/mgR} (n=6) and SMKO-Fbn1^{mgR/mgR} (n=5) mice (males). Scale bar = 100 μm. Quantitation in graph; $p = 0.01$ WT vs Fbn1^{mgR/mgR}; $p = 0.003$, Fbn1^{mgR/mgR} vs SMKO-Fbn1^{mgR/mgR}, Kruskal-Wallis non parametric test with Dunn's multiple comparisons test. IgG, rabbit IgG used as negative control.

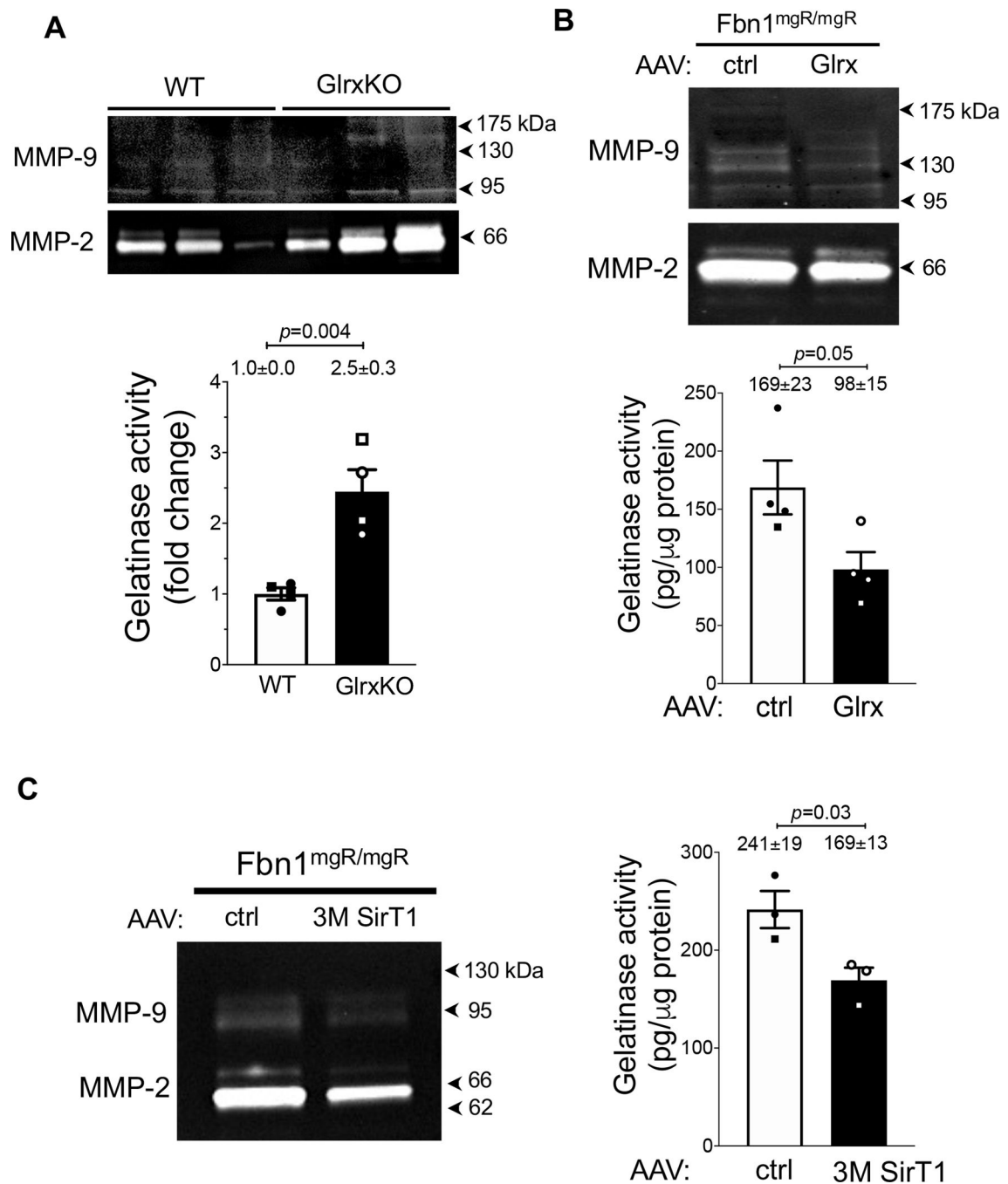


Figure 7.

(A) Representative images of MMP activity, measured using in-gel zymography, in cell culture medium from WT and Glrx knockout (GlrxKO) VSMCs. Band intensities are normalized to 10 ng of recombinant MMP2, which was used as a standard (*not shown*) and expressed as average fold-change of pg gelatinase activity per μg protein. n=4 replicate experiments with VSMCs isolated from 4 WT and 4 GlrxKO mice (*circles*, females; *squares*, males); $p=0.004$, unpaired Student's t-test. (B) In-gel zymography in medium of Fbn1^{mgR/mgR} VSMCs treated with a control AAV or an AAV overexpressing Glrx.

n=4 replicate experiments with VSMCs isolated from 8 female (*circles*) or male (*squares*) Fbn1^{mgR/mgR} mice; $p=0.05$, Mann-Whitney non parametric test. (C) Representative images of MMP activity, measured using in-gel zymography, in medium of Fbn1^{mgR/mgR} VSMCs infected with a control or 3M SirT1 AAV. n=3 replicate experiments with VSMCs isolated from 6 female (*circles*) or male (*squares*) Fbn1^{mgR/mgR} mice; $p=0.03$, unpaired Student's t-test.

Author Manuscript

Author Manuscript

Author Manuscript

Author Manuscript

Table 1.

Table summarizes the incidence of TAA and aortic enlargements in WT (n=40) and Marfan (Fbn1^{mgR/mgR}; n=50) mice; male (M) and female (F) subgroups are indicated. Aortic enlargements are defined as aortic diameters larger than WT, but not yet at the threshold of >150% initial diameter to be considered AA.

	WT (M)	WT (F)	Fbn1 ^{mgR/mgR} (M)	Fbn1 ^{mgR/mgR} (F)
Number of mice (n)	40		50	
Sex subgroups (n)	25	15	28	22
Age (months)	4.2 ± 0.2		4.5 ± 0.2	
TAA + enlargement (%)	0 (0%)		28 (90%)	
	0 (0%)	0 (0%)	14 (100%)	14 (82%)